Nuclear Structure Studies at ISOLDE and their Impact on the Astrophysical r-Process

Karl-Ludwig Kratz [a] Bernd Pfeiffer [a] Friedrich-Karl Thielemann [b]
William B. Walters [c]

[a] *Institut für Kernchemie, Universität Mainz, Germany*
E-mail: klkratz@vkcmzd.chemie.uni-mainz.de
[b] *Departement für Physik und Astronomie, Universität Basel, Switzerland*
E-mail: fkt@quasar.physik.unibas.ch
[c] *Department of Chemistry, University of Maryland, USA*
E-mail: ww3@umail.umd.edu

The focus of the present review is the production of the heaviest elements in nature via the r-process. A correct understanding and modeling requires the knowledge of nuclear properties far from stability and a detailed prescription of the astrophysical environment. Experiments at CERN/ISOLDE have played a pioneering role in exploring the characteristics of nuclear structure in terms of masses and β-decay properties. Initial examinations paid attention to far unstable nuclei with magic neutron numbers related to r-process peaks, while present activities are centered on the evolution of shell effects with the distance from the valley of stability. We first show in site-independent applications the effect of both types of nuclear properties on r-process abundances. Then, we explore the results of calculations related to two different 'realistic' astrophysical sites, (i) the supernova neutrino wind and (ii) neutron star mergers. We close with a list of remaining theoretical and experimental challenges needed to overcome for a full understanding of the nature of the r-process, and the role CERN/ISOLDE can play in this process.

Keywords: nuclear astrophysics, r-process nucleosynthesis, isotope and isomer separation via HF splitting, Laser ion source, nuclear structure, neutron-rich isotopes, ultra-metal-poor halo stars

1. Introduction

The astrophysical rapid neutron-capture process (r-process) has been recognized for a long time as the scenario responsible for the synthesis of approximately half of the nuclear species in nature, which are more massive than Fe [1,2]. It requires environments with a high neutron density, where neutron captures are faster than β-decays, even for neutron-rich unstable nuclei up to 15-30 units from stability. Only under such conditions it is possible that highly unstable nuclei are produced near the neutron drip-line via neutron captures, (γ, n)-photodisintegrations, β^--decays and β-delayed processes, leading also to

the formation of the heaviest elements in nature like Th, U, and Pu. Far from stability, magic neutron numbers are encountered for smaller mass numbers A than in the valley of stability, which shifts the r-process abundance peaks in comparison to the s-process peaks (which occur at neutron shell closures at the stability line due to small neutron capture cross sections). Besides this basic understanding, the history of r-process research has been quite diverse in suggested scenarios (for reviews see [3–10]). Starting with a seed distribution somewhere around A=50-80 before massive neutron-capture sets in, the operation of an r-process requires 10 to 150 neutrons per seed nucleus to form all heavier r-nuclei. The question is which kind of environment can provide such a supply of neutrons to act before decaying with a 10 min half-life. The logical conclusion is that only explosive environments, producing or releasing these neutrons suddenly, can account for such conditions. Without having discussed any stellar models yet, we want to mention some recent literature on these issues. The r-process site is not a settled one; however, two astrophysical settings are suggested most frequently: (i) Type II supernovae (SNII) with postulated high-entropy ejecta [11–13], where the delayed emergence of r-process matter in galactic evolution [14,15] indicates that these can probably only be SN with small progenitor mass; and (ii) neutron star mergers or other events with low-entropy ejecta [16–19].

1.1. Equilibria in Explosive Burning

After this ad hoc introduction of sites, we want to return first to the conditions in high-temperature explosive plasmas in order to test what kind of nuclear-physics input is required, and also what type of thermodynamic environment properties can lead to the neutron to seed ratios mentioned above. The main aspect is that a whole variety of burning processes responsible for the abundances of intermediate and heavy nuclei, like e.g. explosive O and Si-burning, are leading to partial (quasi) or full equilibria of reactions (QSE or NSE). These are described by the chemical potentials of nuclei which form a Boltzmann gas. The abundance ratios are (besides thermodynamic environment properties) determined by mass differences. Therefore, mass uncertainties matter, while uncertainties in cross sections do not enter abundance determinations. Non-equilbrium regions are identified by small reaction cross sections, either due to small Q-values for reactions out of the magic numbers or due to small level or resonance densities for light nuclei. For sufficiently high temperatures all QSE groups merge to a full NSE.

The chemical equilibrium for neutron or proton captures leads to abundance maxima at specific neutron or proton separation energies

$$\frac{Y(A_c)}{Y(A_t)} = n_p \frac{G(A_c)}{g_p G(A_t)} \Big[\frac{A_c}{A_p A_t}\Big]^{3/2} \Big[\frac{2\pi\hbar^2}{m_u kT}\Big]^{3/2} \exp(S_p(A_c)/kT) \qquad (1)$$

$$\frac{S_p(A_c)}{kT} = 24 \ln\Big[(\frac{A_t A_p}{A_c})^{3/2}(\frac{G(A_t)g_p}{2G(A_c)})^{3/2}(\frac{T}{10^9\mathrm{K}})^{3/2}\frac{N_A}{n_p/\mathrm{cm}^3}\Big]. \qquad (2)$$

These equations are valid for neutron, proton and/or α captures, as indicated by the subscript p (projectile); subscript t stands for target and c for the compound nucleus. The Y's are abundances related to number densities n via $n = \rho N_A Y$, where ρ denotes the mass density and N_A the Avogadro number. At the maximum in an isotopic or isotonic line we have $S_{p=n \text{ or } p} \approx 24kT$, if the partition functions G are neglected. This is slightly modified by logarithmic dependences on projectile (neutron or proton) density n_p and temperature T. In case an equilibrium with neutrons and protons exists, the abundance maximum is found in the nuclear chart at the intersection of the relevant neutron and proton separation energies. The free neutron and proton densities reflect the total neutron/proton ratio in matter, which is determined by slow (not in equilibrium), weak interactions via changing the total proton/nucleon ratio $Y_e = <Z/A>$.

The understanding that explosive burning stages are governed by QSE or even NSE is growing [20–22,9]. This has been shown recently in calculations of SNII nucleosynthesis [23,24] with two different libraries of nuclear reaction rates. Different types of QSE-groups can emerge in explosive burning. The high temperature phase of the rp-process (rapid proton capture) in X-ray bursts, where no neutrons are available, witnesses isotonic lines in a $(p,\gamma) \rightleftharpoons (\gamma,p)$ equilibrium [25,26]. Another application is the r-process, the focus of the present paper. Here the QSE-groups are isotopic lines in an $(n,\gamma) \rightleftharpoons (\gamma,n)$ equilibrium. The connecting weak interactions for both processes are β^+- or β^--decays. During the final freeze-out from equilibria, when temperatures decline below equilibrium conditions, reaction rates and capture cross sections can count again. In general, it should be pointed out that equilibria simplify the understanding of explosive nucleosynthesis processes and individual cross sections play a much less important role than reaction Q-values. Since the rp- and r-process explore exotic nuclei close to the proton or neutron drip-lines, we need to focus on nuclear masses and β-decay properties. An understanding of the underlying nuclear structure is essential for both types of nuclear parameters. Such information usually comes from a close interplay between experiment and theory. This will be discussed in more detail in sections 3 and 4.

1.2. Necessary Environment Properties for r-Process Nucleosynthesis

In order to underline why (within an understanding of the - nuclear - functioning of the r-process) the two scenarios mentioned in the beginning of this section seem to be the most promising ones, we want to present here two major results found recently by Freiburghaus et al. [13]. They performed an analysis of neutron to seed ratios in different types of adiabatic expansions with a given entropy S, proton/nucleon ratio Y_e, and expansion time scale. In order to obtain the required 10 to 150 neutrons per r-process seed nucleus (in the Fe-peak or

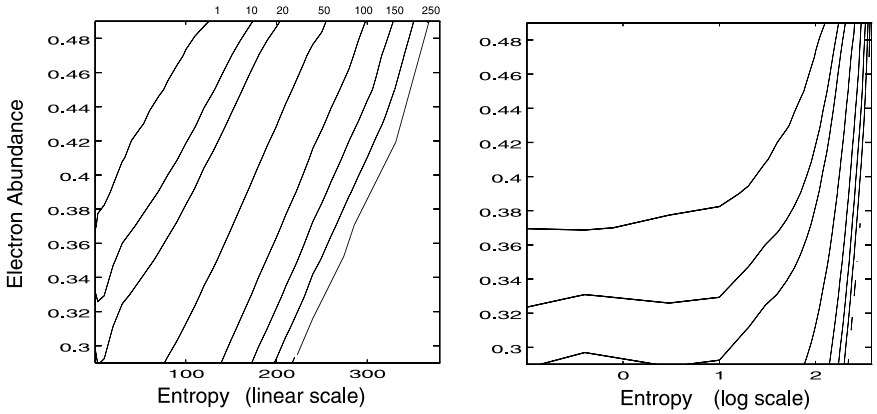

Figure 1. Y_n/Y_{seed} contour plots as a function of intial entropy S and electron abundance Y_e for an expansion time scale of 0.05s. The left part shows how, for moderate Y_e-values, an increasing neutron/seed ratio - indicated by contour lines labeled with the respective Y_n/Y_{seed} – can be attained with increasing entropy. The results scale with Y_e, measuring the global proton/nucleon ratio. The right part of the figure enhances on a logarithmic scale the low-entropy behaviour, where Y_n/Y_{seed} is only determined by Y_e. The contour lines are the same for both figures.

somewhat beyond) permitting to produce nuclei with masses A>200, this translates into a $Y_e = <Z/A> = 0.12$–0.3 for a composition of Fe-group nuclei and free neutrons. Such a high neutron excess is only available for high densities in neutron stars under β-equilibrium ($e^- + p \leftrightarrow n + \nu$, $\mu_e + \mu_p = \mu_n$), based on the high electron Fermi energies which are comparable to the neutron-proton mass difference [17].

Another option is a so-called extremely α-rich freeze-out in complete Si-burning with moderate Y_e>0.40. This corresponds to a freeze-out from QSE with a weak connection between the light (n, p, α) and heavy (Mg–Kr) QSE groups due to low densities. The links accross the particle-unstable A=5 and 8 gaps are only possible via the three-body reactions $\alpha\alpha\alpha$ and $\alpha\alpha n$ to ^{12}C and ^{9}Be, whose reaction rates show a quadratic density dependence. The entropy can be used as a measure of the ratio between the remaining He mass-fraction and heavy nuclei. Similarly, the ratio of neutrons to heavy nuclei (i.e. the neutron to seed ratio) is a function of entropy and permits for high entropies, with large remaining He and neutron abundances compared to small heavy-seed abundances, neutron captures which proceed to form the heaviest r-process nuclei [27,12,11,28,29]. After the freeze-out of charged-particle reactions in matter, which expands from high temperatures but relatively low densities, as much as 90% of all matter can be locked into ^{4}He with N=Z, which leaves even for moderate Y_e's a large neutron/seed ratio for the few existing heavier nuclei.

The behaviour of these two environments, representing a normal (low-entropy) and an α-rich (high-entropy) freeze-out, is summarized in Fig. 1. The

available number of neutrons per heavy nucleus Y_n/Y_{seed} after charged-particle freeze-out, when the large QSE-groups break up into isotopic lines, is shown as a function of entropy and initial Y_e. At low entropies the transition to a normal freeze-out occurs, indicated by the negligible entropy dependence.

This introduction centered (in a cursory way) on the questions: (i) How can one obtain - after an expansion and cooling to temperatures of $2-3\times10^9$K, when the charged-particle freeze-out occurs - the neutron to seed ratios required for a successful r-process; and (ii) what type of nuclear-physics input is of dominant importance. In the following section 2, we will discuss in more detail the methods to follow abundance changes during the neutron-capture phase, and will show how in simplified r-process models the observed abundance features and nuclear properties far from stability are related. In section 3, we present the nuclear-data input employed, and show the strong effects which the choice of nuclear data can have. Section 4 summarizes the experimental information on r-process nuclei, to a large extent obtained at CERN/ISOLDE. Finally, in section 5 we discuss how r-process calculations evolved over the past decade with continuously improved nuclear-structure knowledge from initially classical equilibrium calculations to recent results from specific astrophysical sites.

2. r-Process Nucleosynthesis Calculations

The system of differential equations for an r-process network includes the terms for neutron captures, neutron-induced fission, photodisintegrations, β-decays, β-delayed neutron emission and fission. This leads to a set of N differential equations for the individual nuclear abundances as in Eq.(3)

$$\dot{Y}(Z,A) = \sum_{Z',A'} \lambda^{Z',A'} Y(Z',A') + \sum_{Z',A'} \rho N_A < \sigma v >_{Z',A'} Y(Z',A') Y_n, \qquad (3)$$

where the first term on the right-hand side includes β-decays (with all possible emission channels, including delayed fission), spontaneous fission, and photodisintegrations. The second term includes all neutron-induced reactions. The terms are positive or negative, depending upon whether they produce or destroy the nucleus (Z,A). For the heavy (i.e. high-Z) and neutron-rich nuclei in question, due to the high Coulomb barriers between the particles only neutron-induced reactions are of importance for the temperatures of interest. Thus, only reactions involving neutrons as projectiles or emitted particles, such as (γ,n)-photodisintegrations and β-delayed neutron emission, need to be considered. We can replace $\rho N_A Y_n$ in Eq.(3) by the neutron number density n_n, underlining the fact that n_n is the important quantity for the r-process rather than the neutron abundance. For nuclei with $Z<80$, fission does not play any role, and neutron captures, photodisintegrations and β-decays (including delayed-neutron branch-

ings) dominate. If we include β-decays leading to the emission of up to three delayed neutrons, the abundance change of nucleus (Z,A) is given by

$$\dot{Y}(Z,A) = n_n Y(Z,A-1)\sigma_{A-1} + Y(Z,A+1)\lambda_{A+1} \quad (4a)$$
$$-Y(Z,A)(n_n\sigma_A + \lambda_A + \lambda_\beta^A + \lambda_{\beta n}^A + \lambda_{\beta 2n}^A + \lambda_{\beta 3n}^A) \quad (4b)$$
$$+Y(Z-1,A)\lambda_\beta^{Z-1,A} + Y(Z-1,A+1)\lambda_{\beta n}^{Z-1,A+1} \quad (4c)$$
$$+Y(Z-1,A+2)\lambda_{\beta 2n}^{Z-1,A+2} + Y(Z-1,A+3)\lambda_{\beta 3n}^{Z-1,A+3}, \quad (4d)$$

where σ_{A-1} is the thermally averaged (n,γ)-reaction rate $\langle\sigma v\rangle$ of nucleus $(Z, A–1)$, λ_{A+1} is the photodisintegration rate (γ,n) for nucleus $(Z, A+1)$, λ_β^A is the β-decay rate of nucleus (Z,A), and $\lambda_{\beta n}^A$, $\lambda_{\beta 2n}^A$, and $\lambda_{\beta 3n}^A$ are the rates of β-decay followed by the emission of one, two or three neutrons, respectively.

Depending upon the specific conditions, either β-decays can be faster than neutron captures and photodisintegrations like in an s-process, or vice versa, when an $(n,\gamma)\rightleftharpoons(\gamma,n)$ equilibrium exists [see sect. 1 and Eq(1)]. If the β-flow (i.e. the β-decays of the nuclei) from each Z-chain to $(Z+1)$ is equal to the flow from $(Z+1)$ to $(Z+2)$, then a steady-flow or β-flow equilibrium will exist. When an $(n,\gamma)\rightleftharpoons(\gamma,n)$ equilibrium or a steady-flow condition is established, Eq.(4) simplifies. With these simplifications, a solution of the general set of equations, which would involve a linear system of the size of a nuclear network, can be avoided.

As long as there is a high neutron density and a large high-energy photon density (i.e. a high temperature), we can expect that neutron captures and photodisintegrations occur on a much faster time scale than β-decays. This leads after charged-particle freeze-out (see sect. 1) to QSE groups in form of isotopic chains (denoted $(n,\gamma)\rightleftharpoons(\gamma,n)$ equilibrium or *'waiting-point'* approximation), where the nucleus with maximum abundance in each isotopic chain must wait for the longer β-decay time scale. The chemical equilibrium $\mu_n + \mu_{Z,A} = \mu_{Z,A+1}$ of particles in a Boltzmann gas causes abundance ratios which are dependent only on n_n, T and S_n

$$\frac{Y(Z,A+1)}{Y(Z,A)} = n_n \frac{G(Z,A+1)}{2G(Z,A)}\Big[\frac{A+1}{A}\Big]^{3/2}\Big[\frac{2\pi\hbar^2}{m_u kT}\Big]^{3/2}\exp(S_n(A+1)/kT). \quad (5)$$

This equation is identical to Eq.(1) with p(projectile)=n, A_p=1, A_t=A, A_c=$A+1$, and g_n=2. The neutron-separation energy S_n introduces the dependence on nuclear masses in an $(n,\gamma)\rightleftharpoons(\gamma,n)$ equilibrium, where the abundance maxima in each isotopic chain are located at the S_n given by Eq.(2), which is the same in all isotopic chains. Fig. 2 shows such a contour line of $S_n\simeq$2MeV for the Finite Range Droplet Model, FRDM [30]. In addition it displays the line of stability and the solar r-abundances as a function of A.

The abundance flow from each isotopic chain to the next is governed by β-decays. We can introduce a total abundance in each isotopic chain

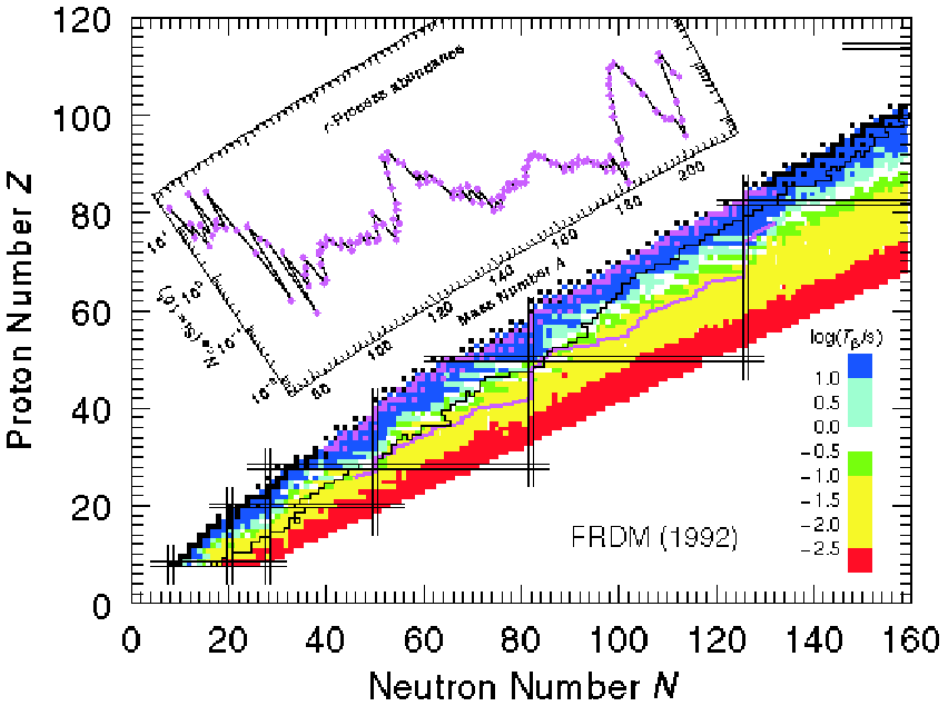

Figure 2. Schematic illustration of the r-process path (dark line on the neutron-rich side of β-stability) and observed r-abundances (insert). Sharp peaks occur near A$\simeq$80, 130, and 195, where the r-process path crosses the N=50, 82, and 126 magic neutron numbers. The chart of neutron-rich nuclides is shaded according to measured and predicted β-decay half-lives, $T_{1/2}$. Grey scales for $T_{1/2}$ ranges are explained in the legend bar.

$Y(Z)$=$\sum_A Y(Z,A)$, and each $Y(Z,A)$ can be expressed as $Y(Z,A)$=$P(Z,A)Y(Z)$. The individual population coefficients $P(Z,A)$ are obtained from the equilibrium condition [Eq.(5)]. The set of differential equations which replaces Eq.(4) in this case is

$$\dot{Y}(Z) = Y(Z-1)\sum_A P(Z-1,A)\lambda_\beta^{Z-1,A} - Y(Z)\sum_A P(Z,A)\lambda_\beta^{Z,A}, \qquad (6)$$

where $\lambda_\beta^{Z,A}$ is the β-decay rate of nucleus (Z,A). This is a system of as many equations as the number of Z-chains. The individual abundances are obtained from Eq.(5).

The waiting-point approximation is only valid for high temperatures and neutron number densities of the gas before the freeze-out from chemical equilibrium with neutrons occurs [31,32]) for neutron number densities and temperatures as low as $n_n\simeq10^{20}$ cm^{-3} and $T\simeq10^9$ K. Process timescales in excess of β-decay

half-lives lead to a steady-flow equilibrium, in addition to an $(n,\gamma)\rightleftharpoons(\gamma,n)$ equilibrium, i.e. $\dot{Y}(Z)$=0 in Eq.(6) or

$$Y(Z)\sum_{A} P(Z,A)\lambda_{\beta}^{Z,A} = Y(Z)\lambda_{\beta}(Z) = \text{const.} \qquad (7)$$

In such a steady-flow equilibrium, the assumption of an abundance for $Y(Z_{min})$ at a minimum Z-value is sufficient to predict the r-process curve. The calculation of $P(Z,A)$ from Eq.(5) requires the knowledge of nuclear masses (or S_n-values), a neutron number density n_n and a temperature T. The β-decay rates in Eqs.(4), (6) and (7) are related to the half-lives of very neutron-rich nuclei via $\lambda_{\beta} = ln(2)/T_{1/2}$. Thus, in the simplest of all cases, i.e. provided that an $(n,\gamma)\rightleftharpoons(\gamma,n)$ equilibrium and a steady-flow has been reached, the knowledge of n_n, T, S_n, and $T_{1/2}$ alone would be sufficient to predict the whole set of abundances as a function of A. Results by Kratz et al. [33–35] indicated that this be the case for conditions which reproduce the low-mass wings of the $A\simeq$80 and $A\simeq$130 peak regions of the solar-system r-process abundances $N_{r,\odot}$ [36,37].

In the most general case of (astrophysical) environment conditions, we have thus to solve the set of Eq.(4) for all nuclei from stability to the neutron drip-line (1000-2000). The type of conditions after charged-particle freeze-out discussed in section 1.2 permits, however, the use of Eq.(6), i.e. the assumption of an $(n,\gamma)\rightleftharpoons(\gamma,n)$ equilibrium. For small β-decay half-lives, encountered in between magic numbers and for small Z's at magic numbers, even the steady-flow approximation of Eq.(7) seems applicable, until the final neutron and temperature freeze-out no longer permits the use of any equilibrium approach. Here, one can imagine two extreme options: (i) The occurance of an instantaneous freeze-out; then the results of Eq.(6) just have to be followed by the final decay back to stability, where also β-delayed properties (neutron emission and fission) are needed. (ii) In the more general case of a slow freeze-out, the set of Eq.(4) has to be solved. Then also neutron captures can affect the initial waiting-point abundance results.

3. Testing Nuclear Physics Models

For testing nuclear-structure properties it is advisable to make use of a simple astrophysical environment model, with n_n=const, T=const and a duration time τ, but chosen for conditions where an equilibrium in isotopic chains is obtained and Eq.(6) can be applied (however, without assuming the steady flow of Eq.(7)). Fig. 3 shows three such calculations for n_n=10^{20}, 10^{22}, and 10^{24} g cm^{-3} at T=1.35×10^9 K for duration times τ of 1.2, 1.7, and 2.1 s, respectively. When testing the resulting abundances, one notices that a steady flow [Eq.(7)] is actually obtained for the low-mass wings of the peaks and the connecting lighter-mass regions between magic neutron numbers. When entering these conditions, which reproduce the three r-process peaks, into Eq.(2), one notices that they correspond to three different r-process paths with different neutron-separation energies S_n

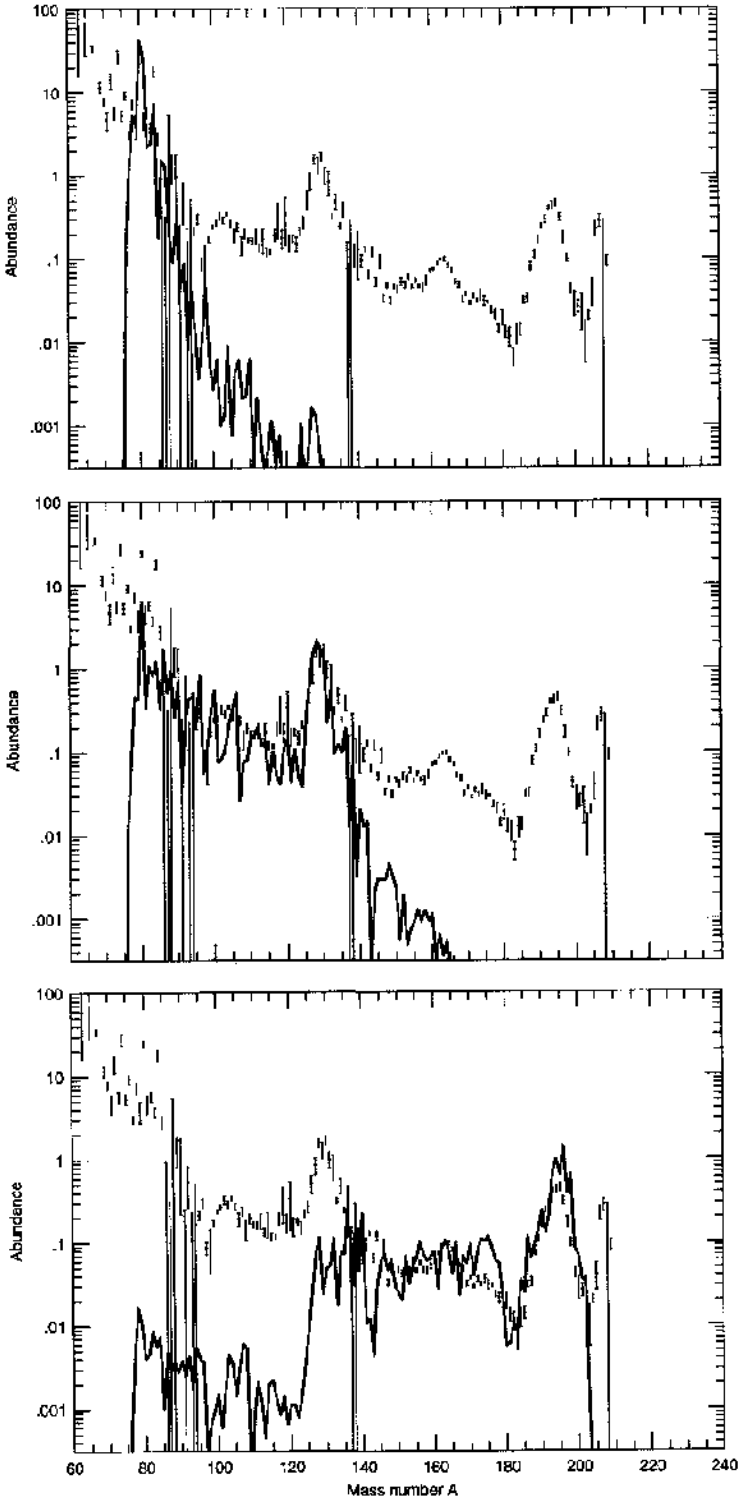

Figure 3. Results of time-dependent r-process calculations with n_n=10^{20}, 10^{22}, and 10^{24} g cm^{-3} at T=1.35×10^9 K for duration times τ of 1.2, 1.7, and 2.1 s, respectively, in comparison with solar r-process abundances [35].

between 4 and 2 MeV. This indicates that a full fit to the solar r-process abundances requires a superposition of different stellar conditions (but not necessarily different astrophysical sites).

3.1. Nuclear Physics Input

As outlined in the previous section, for a given neutron density (or radiation entropy), the r-process proceeds along a contour line of constant S_n to heavier nuclei (see, e.g. Fig. 4 in [38], where the abundance flow from each isotopic chain to the next is dominated by the β-decays. The flow equilibrium then implies approximate equality of progenitor abundance $N_{r,prog}$ (i.e. the initial abundance of a waiting-point isotope lying in the r-process path) times β-decay rate λ_β. Thus, with $N_{r,prog}(Z)\lambda_\beta(Z)$=const. the half-lives along the r-process flow path would directly define the $N_{r,prog}$, and – when taking into account P_n branching during freeze-out – also the final $N_{r,\odot}$. Still some 15 years ago, there were severe doubts among astrophysicists that the validity of this simple and elegant approximation would ever be proven, because it requires experimental information on far-unstable waiting-point isotopes believed to be inaccessible in terrestrial laboratories. However, only a few years later in 1986, a new area in nuclear astrophysics started with the identification of the first two classical neutron-magic waiting-point isotopes $^{130}Cd_{82}$ at CERN/ISOLDE [39], and $^{80}Zn_{50}$ at the fission-product mass separators OSIRIS [40] and TRISTAN [41]. As was shown by Kratz et al. [39,33,34], indeed, first evidence for the existence of – at least a local – steady-flow equilibrium could be achieved, which presented a stimulating challenge to both theoreticians and experimentalists in the nuclear-physics community in the following years.

Nevertheless, even today the vast majority of very neutron-rich r-process nuclei is experimentally not accessible. Therefore, a general understanding of their nuclear properties remains to be obtained only through theoretical means. Since a number of different quantities are needed in r-process calculations, as outlined above, in the past it was often not possible to derive them all from one source. Taking them from different sources, however, may raise the question of consistency. In order to avoid an eventual vanishing of real signatures or the creation of artificial r-abundance effects from the use of nuclear-physics parameters from different models – sometimes even of largely different sophistication – we have performed our r-process calculations in a unified macroscopic-microscopic approach in which all nuclear properties can be studied in an internally consistent way. This approach is, for example, discussed in detail in Kratz et al. [35] and Möller et al. [42] for the combination of nuclear masses from the Finite Range Droplet Model, FRDM and β-decay properties from a Quasi-Particle Random Phase Approximation, QRPA [43], in its present version using Folded-Yukawa single-particle levels and the Lipkin-Nogami pairing model (Möller and Randrup [44]). Analoguously, when adopting other mass formulae, such as the Extended

Thomas-Fermi plus Strutinsky Integral models, ETFSI-1 (Aboussir et al. [45]) or ETFSI-Q (Pearson et al. [46]), or the spherical Hartree-Fock-Bogolyubov method with a specific Skyrme force, HFB/SkP (Dobaczewski et al. [47,48]), we normally use theoretical β-decay quantities deduced from QRPA calculations with masses and deformation parameters given by that particular model.

With the above macroscopic-microscopic approaches, several rather sophisticated and internally consistent, global nuclear-data sets are now available for astrophysical calculations which are expected to yield more reliable predictions than earlier models, like the old droplet-type formulae of Myers [49] and Von Groote et al. [50] or the Gross Theory of β-decay (Takahashi et al. [51]). Nevertheless, being aware that even the more microscopic approaches do have their deficiencies, we have continuously tried to improve the basic data sets by short-range extrapolations of known nuclear-structure properties, either model-inherently not contained in or not properly described by the above global methods. For details, see e.g. Kratz et al. [35]. And, in contrast to other authors who prefer to use exclusively model predictions in their r-process calculations (see, e.g. [32]), we have steadily updated our files by including all new experimental masses, $T_{1/2}$ and P_n values ([52,53]).

These nuclear-data sets have been used extensively during the last years in our r-process calculations ([35,38,54–58,13]) to reproduce the $N_{r,\odot}$ pattern [36,37] and to test nuclear structure close to the neutron drip-line.

3.2. Testing Nuclear Physics Models

As has been outlined in sect. 2, calculated r-abundances are strongly dependent on model predictions of masses and β-decay properties. Therefore, it seems worthwhile to test the influence of the choice of nuclear theories in selected mass regions before performing global, multi-component r-process calculations. Such tests may well be able to shed some light on the development of nuclear structures towards the neutron drip-line, and with this may define certain key properties and key experiments. Of particular importance in this context are the $N_{r,\odot}$ peak areas, since the related N=50, 82 and 126 shell closures act as 'bottle necks' for the r-process matter flow.

Already Burbidge et al. [1] pointed out that the r-process very likely passes through neutron-magic isotopes around A$\simeq$80, 130 and 195 which have longer-than-average β-decay half-lives. At these points the r-abundances build up and form the observed $N_{r,\odot}$ peaks, as nuclei like $^{80}Zn_{50}$, $^{130}Cd_{82}$ and $^{195}Tm_{126}$ 'wait' to β-decay. It is therefore immediately evident that these clasical 'waiting points' would not only give important constraints on r-process conditions, but would also yield much needed information on shell struture far from β-stability.

In fact both, the 'long' $T_{1/2}$ of the above three classical waiting-point nuclei, as well as the 'low' S_n values of the respective (N_{mag}+1) isotopes will considerably slow down the nuclear flow through the A$\simeq$80, 130 and 195 mass regions, and

with this will to a large extent determine the total duration of a 'canonical' r-process [1,6,34]. To first illustrate this for the β-decay half-lives, Fig. 4 shows four calculations of an r-process component mainly responsible for the build-up of r-abundances in the A$\simeq$130 peak region, where all stellar (T_9, n_n, τ) and nuclear-physics (Q_β, S_n, ϵ_2, P_n) input parameters (taken from [30,52,53]), except the β-decay half-lives of $^{129}Ag_{82}$ and $^{130}Cd_{82}$, are kept constant. The $T_{1/2}$ of these two waiting-point isotopes are varied within the range of earlier model predictions. It is quite evident from this figure, that the $T_{1/2}$ not only determine the height (and shape) of the A$\simeq$130 $N_{r,\odot}$ peak, but also the r-matter flow to higher masses. With 'short' half-lives ($T_{1/2}$=20 ms; see upper left part of Fig. 4), the r-process would pass the N=82 region more or less unhindered; this would result in a 'short' overall process duration. On the other hand, 'long' half-lives ($T_{1/2}$=750 ms; see lower right part of Fig. 4) would slow down the nuclear flow through the A$\simeq$130 region considerably, and consequently would require an r-process duration of 5–10 s when starting from Z=26. Such time scales are, however, too long for the presently favoured r-process scenarios. With this, also the reliability of gross β-decay theories which yield model-inherently 'longer' $T_{1/2}$ far from stability [51,59], may be questioned.

We now want to test the behaviour of different mass models; i.e. the old Hilf et al. formula [60], the two global macroscopic-microscopic theories FRDM [30] and ETFSI-1 [45], and the recent microscopic spherical HFB+SkP model [61]. Within a very simple *static* approximation (see, e.g. [33,35]), one can obtain a first rough estimate under which neutron-density conditions an r-process will start to break through the classical waiting points at N=50, 82 and 126. As can be seen from Fig. 5, depending on the magic shell there are considerable differences for the four mass models chosen. The behaviour is clearly correlated with the respective shell strengths. A strong shell closure is reflected by a low neutron separation energy (in Fig. 5 given as $\overline{S}_n$=[S_n(A)+S_n(A+1)]/2) and a high neutron density required to overcome the neutron-capture 'bottle-necks' at ^{80}Zn, ^{130}Cd and ^{195}Tm. When focussing for example on N=82, the strongest shell closure is predicted by the ETFSI-1 model, whereas the recent HFB+SkP indicates a much weaker magicity. Already from this simple picture it is evident, that for the production of the whole $N_{r,\odot}$ distribution quite different neutron-density regimes will be required for different mass models.

In a next step, we will check the above indication by more realistic time-dependent calculations. In Fig. 6, the results of four one-component r-process calculations are shown, which use exactly the same astrophysical parameters as in our $T_{1/2}$ test to produce the A$\simeq$130 r-abundance region (see Fig. 4). In all calculations, the β-decay properties were now taken from our recent evaluation [53]. In this picture, the decisive nuclear-physics quantity are the S_n values, in particular those of the waiting-point isotopes before and at N=82. Apart from a certain memory effect from the N=50 shell closure, it is quite obvious that the predicted N=82 shell strength (see Fig. 5) determines the r-matter flow in

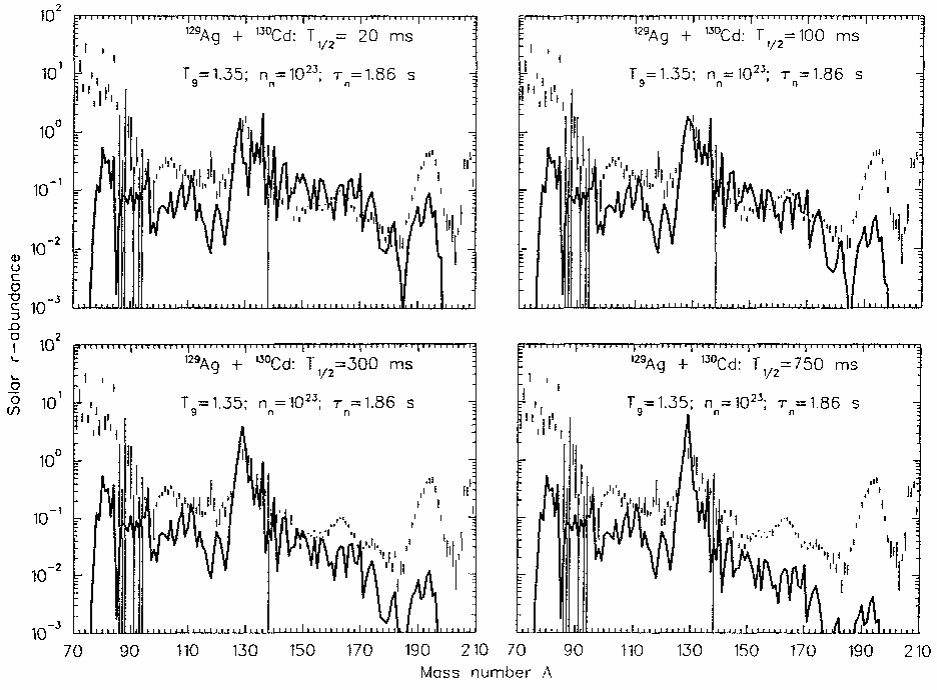

Figure 4. Time-dependent calculations of an r-process component which is mainly responsible for the build-up of abundances in the A≃130 region. All stellar and nuclear-physics input parameters, except the β-decay half-lives of the two N=82 waiting-point isotopes ^{129}Ag and ^{130}Cd, are kept constant. For details, see text.

the A≃130 peak region and beyond. For mass models with a pronounced N=82 shell closure, i.e. FRDM and ETFSI-1, a significant r-abundance trough occurs around A≃115, and the low S_n's of the N=83 isotones of $_{41}$Nb to $_{48}$Cd prevent a rapid matter flow to heavier masses under the given astrophysical conditions. On the other hand, a weaker N=82 shell closure, as e.g. predicted by the Hilf et al. formula and the recent HFB/SkP theory, allows a more rapid build-up and transit of the A≃130 region. With these mass models, the N=82 magic shell is reached at a higher Z (i.e. not before $_{43}$Tc), thus avoiding the A≃115 abundance deficiency. And, at the same time, due to their somewhat higher S_n(N=83) values the break-out from N=82 can occur already at a lower neutron density (i.e. around n_n≃1–5×10^{22} cm^{-3}, according to Fig. 5). We see from Fig. 6, that in the 'extreme' of the HFB/SkP theory with Bogolyubov-enhanced shell-quenching towards the neutron drip-line, a neutron density of n_n≃10^{23} cm^{-3} and a time scale of τ≃1.9 s are already sufficient to drive the nuclear flow from Fe up to the A≃195 r-abundance peak, whereas with the FRDM and ETFSI-1 mass models just the A≃130 peak is built up. This result may be of particular interest for the recently favoured high-entropy bubble scenario of a type-II supernova [27,62,12],

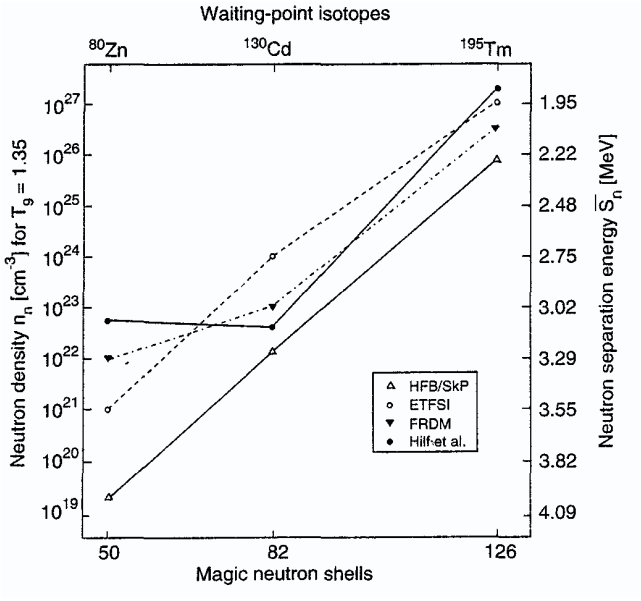

Figure 5. Static equilibrium calculations of n_n conditions for the break-through of an r-process at the classical waiting-point isotopes $^{80}Zn_{50}$, $^{130}Cd_{82}$ and $^{195}Tm_{126}$ for a stellar temperature of T_9=1.35. The four mass models chosen [60,30,45,61] show a different behaviour. Depending on the strength of the shell closure, the break-through occurs at lower n_n (e.g. at N=50, already around $n_n \simeq 10^{19}$ cm^{-3} for the "quenched" HFB/SkP masses) or at higher n_n (again at N=50, only at $n_n \simeq 10^{23}$ cm^{-3} for the Hilf et al. masses). The differences in n_n are correlated with different r-process paths, as indicated by the different average $\overline{S}_n$ values at the right-hand axis of ordinates.

which still encounters some problems in obtaining high enough neutron densities (respectively radiation entropies) to completely build up the A$\simeq$195 r-abundance peak.

4. Experimental information on r-process nuclei

The experimental study of neutron-rich nuclides lying in and near the projected r-process path serves two purposes, provision of direct data for use in nucleosynthesis calculations, and testing the theories from which nuclear properties of far-unstable isotopes are derived when no data are available. As is infered from the nucleosynthesis snapshots shown in the previous section, the predictions of the presently existing global nuclear models quite obviously differ considerably when approaching the limits of particle binding. The reason may well be that the model parameters used so far, which were mainly determined to reproduce known properties near β-stability, need not always be proper to be used at the drip-lines. Therefore, experiments very far from stability will be essential to verify possible nuclear-structure changes with isospin, and to motivate improvements in nuclear

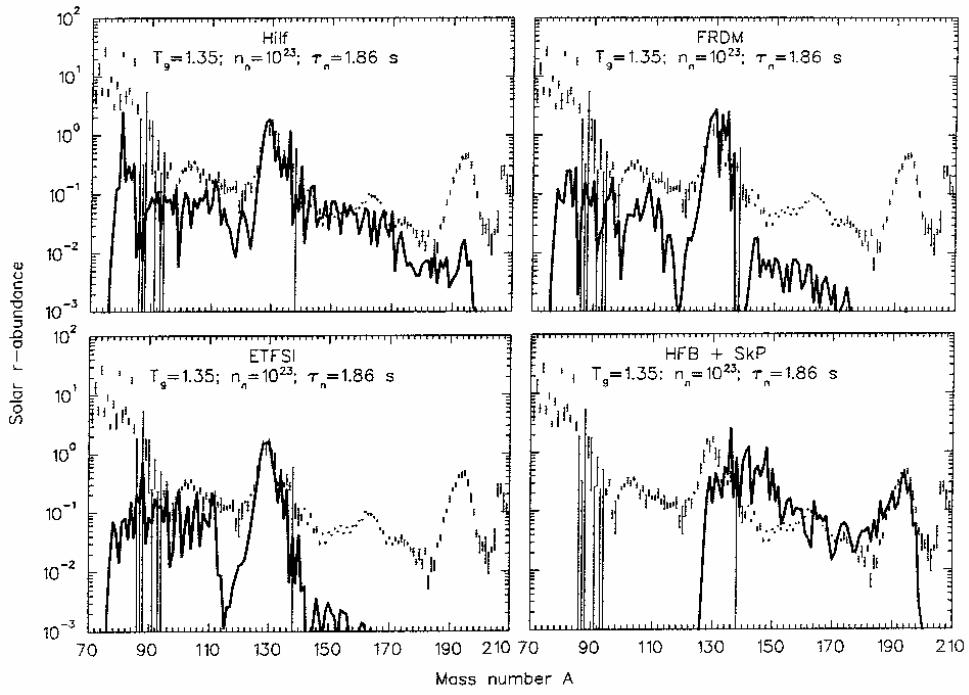

Figure 6. Time-dependent calculations of an r-process component with S_n values from four different mass models [60,30,45,48]. The astrophysical parameters T_9, n_n and τ are the same as in Fig. 4; all nuclear-physics data are taken from [53]. In this picture, the nuclear flow into the A≃130 abundance peak and the mass region beyond is determined by the strength of the N=82 shell, reflected here by the S_n values of the N=81 and 83 isotones of $_{41}$Nb to $_{48}$Cd (see, e.g. Fig. 4 in [54]). For further discussion, see text.

theories.

As already mentioned in sect. 3, only about a decade ago the area of experiments *in the r-process path* started with the identification of the first two classical, neutron-magic 'waiting-point' isotopes: $^{80}Zn_{50}$ (situated 10 mass-units away from stability) and $^{130}Cd_{82}$ (even 16 units beyond stable ^{114}Cd) [40,41,39].

In the following, we will give some technical details on the identification of ^{130}Cd, in order to convince also outsiders from our particular field that such, in principle quite simple experiments are not at all 'easy'. Neutron-rich Cd isotopes were produced at that time at the old CERN/ISOLDE mass separator connected to the 600-MeV proton Synchro-Cyclotron. In this experiment, a UC_2 target in a graphite-cloth matrix was connected to a plasma-discharge ion source via a heated quartz tansfer line. This tube was assumed to serve as a kind of thermochromatography column allowing preferential extraction of volatile species, whereas non-volatile elements should be retained. In this way, some chemical selectivity was intruduced to the otherwise non-selective plasma ionization. Nev-

ertheless, at A=130 strong isobaric contaminations of ^{130}In and ^{130}Cs were observed which made β- and γ-spectroscopy of the orders of magnitude weaker produced ^{130}Cd impossible. Moreover, even with the selective detection method of β-delayed neutron (βdn) counting, the occurrence of – a priori unexpected – $[^{40}CaBr]^+$ molecular ions, at A=130 containing the 1.9-s ^{90}Br βdn-precursor, severely complicated the experimental conditions. To optimize the detection conditions for the searched ^{130}Cd, data from about 36,000 growth (300 ms collections) and decay (900 ms) cycles were accumulated. A careful analysis of the resulting complex βdn-multiscaling curves [39,34] yielded – after subtraction of the ^{90}Br βdn-component – an estimate of the ^{130}Cd half-life between maximum 230 ms (presumably representing a $T_{1/2}$ mixture of Cd-mother and In-daughter decays) and 160 ms (derived from the growth curve during activity collection, where the Cd signals should be enhanced compared to the In-daughter activity).

After all these experimental difficulties, it was quite satisfying to see that our experimental half-life value of (195±35) ms turned out to be in reasonable agreement with the $N_{r,\odot}(Z)\times\lambda_\beta(Z)\approx$const. waiting-point expectation of (180±20) ms, derived independently at that time by Hillebrandt (see, Kratz, Thielemann, Hillebrandt et al. [33]). The correlation found between the ^{131,133}In and ^{130}Cd half-lives and the observed solar abundances of their stable isobars, which was for the first time exclusively based on experimental numbers, immediately became very important to constrain the equilibrium conditions of an r-process. And this success strongly motivated further experimental and theoretical nuclear-structure investigations, as well as astrophysical r-process studies [35,38]. For example, at ISOLDE the second N=50 waiting-point isotope ^{79}Cu could be identified – again using a chemically non-selective plasma-ion source [63]; experimentally known strong P_n branches were shown to be the nuclear-structure origin of the odd-even staggering in the A$\simeq$80 $N_{r,\odot}$ peak [64]; and from the interpretation of the ^{80}Zn decay scheme in terms of $J^\pi=1^+$, two-quasi-particle (2QP) configurations, evidence for a vanishing of the spherical N=50 shell closure far from stability was obtained [65].

Since the late 1980's, considerable progress has been achieved in the study of neutron-rich medium- to heavy-mass nuclei at various laboraties, with ISOLDE always playing a leading role in this field. However, due to the generally very low production yields, the occurrance of isobar, multi-charged ion and molecular-ion contaminations from chemically non-selective ionization modes, or because of the application of non-selective detection methods, *direct* information on isotopes lying in the r-process path(s) could be obtained but in a few exceptional cases. From the majority of investigations, originally dedicated to study nuclear-structure developments as a function of isospin, only *indirect* – but nevertheless also important – information for r-process calculations can be deduced (see, e.g. [34,35,38,54–56]). In this context, we would like to remind the reader of the fascinating phenomenon of the *sudden onset and saturation of ground-state deformation at N=60* (see, e.g. [66–68]), which had in fact led to the first 'astrophysical

request' of N=82 shell quenching [35].

Because of the severe experimental problems to identify r-process nuclei, recent progress has undoubtedly benefitted from the **selectivity** in their production and detection, by applying e.g. Z-selective laser ion-source (LIS) systems, isobar separation or multifold-coincidence techniques.

Today, there are mainly three mass regions, where nuclear-structure information is of particular astrophysical interest. The first is the seed region of the classical r-process which involves very neutron-rich Fe-group isotopes up to the double-magic nucleus ^{78}Ni. We will discuss recent studies in that mass-region in subsect. 4.1. The second region of interest is that of far-unstable isotopes of refractory elements (Zr to Pd) around A$\simeq$115. Here, most r-process calculations show a pronounced r-abundance *trough*, which is believed to be due to deficiencies at and beyond N=72 mid-shell (see, e.g. [35,54,56]. Recent experimental information using chemical separation procedures, or ion-guide and projectile-fragmentation techniques combined with mass separation can, for example be found in [68–72]. The third region of strong nuclear-structure and astrophysics interest is that around the double-magic nucleus ^{132}Sn, which we will discussed in subsect. 4.2.

4.1. The ^{68}Ni region

Recent spectroscopic studies around the double (semi-) magic ^{68}Ni (Z=28, N=40) at LISOL in Louvain-la-Neuve, at GANIL/LISE in Caen and also at CERN/ISOLDE (see, e.g. [73–76], and references therein), have revealed new structure features which are not easy to reconcile with established shell-model calculations in the neutron-rich region between ^{48}Ca and ^{78}Ni. Most (but not all) of the models find that N=40 is a good closed subshell and predict near-zero deformation for neutron numbers in its vicinity. Of course, these ideas are supported by existing data for $_{28}$Ni, $_{30}$Zn, $_{32}$Ge and $_{34}$Se isotopes for which there is a slight peak in the 2^+ energies for N=38 and / or the supposed subshell at N=40, and then a gentle drop in E(2^+) beyond N=42 as the $\nu g_{9/2}$ orbitals fill and some collectivity is observed (see Fig. 7).

However, recent experiments at the PS-Booster ISOLDE using the high Z-selectivity of laser ionization have made possible decay-studies of very neutron-rich $_{25}$Mn isotopes, and the determination of detailed nuclear-structure information for their $_{26}$Fe-daughters. In particular, it was found that – contrary to expectations – the N=40 isotone ^{66}Fe, situated only one proton-pair below double (semi-) magic ^{68}Ni, is already relatively deformed. From the well-known relationship between E(2^+), B(E2) values and collectivity [77], we deduce a deformation value of $\beta_2\simeq$0.26 for ^{66}Fe. As can be seen from Fig. 7, this trend toward collectivity below ^{68}Ni is already observed for ^{64}Fe$_{38}$ with $\beta_2\simeq$0.18. Needless to say, these data serve as an indication that 'theoretical consensus' for sphericity in N=40 isotones with Z<28 does not provide a good description of the structure, and

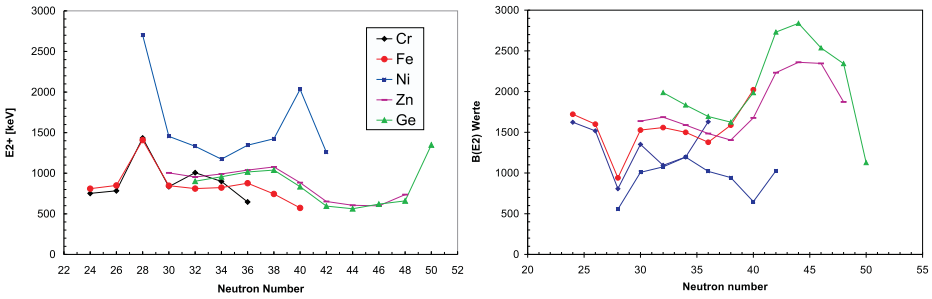

Figure 7. Energies of the first 2^+ levels and B(E2) values of even-even $_{24}$Cr to $_{32}$Ge nuclides.

consequently also of nuclear masses and decay properties of these nuclides. Subsequent data from the GANIL/LISE spectrometer [78,79] in this mass region are in support of our conclusion that the N=40 and adjacent nuclides below ^{68}Ni are relatively deformed, with the maximum collectivity presumably centered around ^{64}Cr$_{40}$. Hence, the use of theoretical results that do not account for deformation of neutron-rich isotopes in this mass region as input data for astrophysical calculations must be approached with caution.

Already with the use of Z-selective laser ionization at the General-Purpose Separator (GPS) of CERN/ISOLDE, it has been possible to study decay properties of 14-ms ^{69}Mn, which is one of the most neutron-rich isotopes with the shortest β-decay half-life beyond the sd-shell. The prospects are good for an extension of such measurements to even heavier isotopes with LIS and the High-Resolution Separator (HRS), eventually including the study of detailed level structures up to ^{70}Fe. Combined with ongoing work on neutron-rich $_{29}$Cu and $_{30}$Zn at ISOLDE and on $_{27}$Co and $_{28}$Ni at other facilities, nuclear-structure information towards the next major neutron-shell closure N=50 will accumulate, to answer e.g. the question about shell-quenching at double-magic ^{78}Ni and its 'bottle-neck' behaviour for the r-process matter flow through N=50. Moreover, the nuclear properties in this region have gained additional importance in the context of the lately discussion of *two* distinct r-process components, a 'weak' r-process below a$\simeq$130, and the 'main' r-process beyond A$\simeq$130 (see sect. 5.2).

4.2. The ^{132}Sn region

The mass region around the far-unstable double-magic nucleus ^{132}Sn has long been and still is of particular interest for experimental and theoretical investigations. Apart from astrophysical importance (formation of the A$\simeq$130 peak of the $N_{r,\odot}$ distribution [35,55]), this region is of considerable shell-structure interest. The neutron-rich isotope $^{132}_{50}$Sn$_{82}$ with its pronounced magicity (only comparable to stable $^{208}_{82}$Pb$_{126}$), together with the properties of the nearest-neighbour single-particle ($^{133}_{\mathbf{51}}$Sb$_{82}$ and $^{133}_{50}$Sn$_{\mathbf{83}}$) and single-hole ($^{131}_{50}$Sn$_{\mathbf{81}}$ and $^{131}_{\mathbf{49}}$In$_{82}$) nu-

clides are essential for tests of the shell model, and as input for any reliable future microscopic nuclear-structure calculations towards the neutron drip-line.

The bulk of the data so far known in this region have been obtained from β-decay spectroscopy at the mass-separator facilities OSIRIS (Sweden) and ISOLDE (see, e.g. [80–87], and references therein). The structures of ^{131}Sn (ν-hole) and ^{133}Sb (π-particle) are fairly well known since more than a decade. More recently, the ν-particle states $2f_{7/2}$ (g.s.), $3p_{3/2}$ (854 keV), $1h_{9/2}$ (1561 keV) and $2f_{5/2}$ (2005 keV), as well as tentatively also the $3p_{1/2}$-particle (1655 keV) and the $1h_{11/2}$-hole ($\approx$3700 keV) states in $^{133}Sn_{83}$ have been identified [80] at the General Purpose Separator (GPS) of the new PS-Booster ISOLDE facility. From these data, valuable information on the spin-orbit splitting of the 2f-orbital and tentatively the 3p-state splitting was obtained. These results were compared to mean-field and HFB predictions, and it was found that none of the potentials currently used in *ab initio* shell-structure calculations was capable of properly reproducing the ordering and spacing of these states (see, e.g. [88], where also possible astrophysical consequences are given). Of particular interest in this context are the surprisingly low-lying $\nu p_{3/2}$- and $\nu p_{1/2}$-states in ^{133}Sn. According to the standard Nilsson model [89], for example, they are expected at 2.89 MeV and 4.36 MeV, respectively. Such lowering of the energies of low-j orbitals (here, by as much as 2.0 MeV and 2.7 MeV, respectively) seems to occur in different mass regions for very neutron-rich nuclides, and has been interpreted, for example, as monopole shifts of single-particle (SP) states[90]. The occurrence of such energy shifts of SP levels has recently also been predicted as a *neutron-skin* phenomenon to occur only near the neutron drip-line (see, e.g. [47]), but not yet in (N_{mag}+1) ^{133}Sn which is still neutron-bound by $S_n \simeq 2.4$ MeV. Nevertheless, following the suggestion of Dobaczewski [47], we have modified the Nilsson potential by reducing the strength of the l^2-term (i.e. the spin-orbit interaction), in order to study its effect on different orbitals. And indeed, this procedure has led to the desired change in the position and even the ordering of the ν-particle states beyond N=82, and has thus allowed at least a qualitative reproduction of the experimental observation of low-lying low-j and high-lying high-j orbitals in ^{133}Sn.

Recently, Zhang et al. [91] have proposed a new set of Nilsson parameters that correctly reproduce the SP levels in ^{131}Sn and ^{133}Sn. They compare their new results with the experimental levels and older Nilsson parameters, as well as SP levels obtained from relativistic mean-field calculations. The danger with this approach is that the change in parameters may be compensating for underlying deficiencies in the model. Consequently, while the results do fit the levels of ^{133}Sn, they may not be useful for astrophysical uses where the goal is to determine the structure of nuclides significantly further from stability.

With these new data, the ^{132}Sn valence-nucleon region is nearly complete. The only missing information are the π-hole states in $^{131}_{\mathbf{49}}$In, which can be studied through β-decay of the very exotic nucleus $^{131}Cd_{83}$. Recent LIS developments

at Mainz [92] and CERN/ISOLDE, using a novel frequency-tripling technique for the Z-selective resonance ionization of Cd, have made possible first test measurements on Cd isotopes in the A≃130 region at the GPS of the PS-Booster ISOLDE. Although the data are not yet fully analyzed, we can already present some interesting new results. For example, the complex βdn-curve at A=130 indicates a half-life component of (162±7) ms on top of the ^{130}In βdn-activity. We assign this component to the r-process waiting-point isotope ^{130}Cd, which we had first identified – using non-selective ionization – with a somewhat longer half-life [39]. As weighted average of the two determinations, we now favour a $T_{1/2}$=(168±12) ms.

In this experiment, it was also possible to measure, for the first time, a half-life for $^{131}Cd_{83}$. The value of (68±3) ms [93] is considerably shorter, and the estimated βdn-branch is much lower than might have been expected. It is possible to estimate a forbidden g.s.-to-g.s. β-branch ($\nu f_{7/2} \rightarrow \pi g_{9/2}$) with a partial half-life of about 120 ms. This means that the Gamow-Teller (GT) allowed decay must also have a half-life of at least 150 ms, as compared to the earlier QRPA prediction of 943 ms [42]. As it is unlikely that the log(ft) value is smaller, this result indcates a significantly larger β-energy driving the GT decay than predicted by the QRPA. In turn, this means either a significantly larger Q_β (meaning a less bound 83^{rd} neutron) or a significantly lower energy for the daughter states to be populated in ^{131}In. Either of these possibilities is an indication that full understanding of the structure of nuclides along the N=82 closed neutron shell is not complete.

In any case, the present results from both detection methods, βdn-counting and γ-spectroscopy, suggest the need of isobar separation, i.e. the use of the HRS at ISOLDE, in order to discriminate the laser-ionized $_{48}$Cd from the unavoidable surface-ionized $_{49}$In isobar.

Another recent study of nuclear-structure development towards N=82 concerns the βdn- and γ-spectroscopic measurements of neutron-rich Ag nuclides at the PS-Booster ISOLDE facility ([84–87,94]), using an improved version of the LIS system described in [95] together with new microgating procedures [96]. This approach was of considerable assistance in minimizing the activities from surface-ionized In and Cs isobars. In this context, the additional 'selectivity' of the spin- and moment-dependent hyperfine (HF) splitting was used to enhance the ionization of either the $\pi p_{1/2}$-isomer or the $\pi g_{9/2}$ g.s.-decay of the Ag isotopes.

The laser response to HF-splitting was calibrated on the stable $J^\pi=1/2^-$ ^{107}Ag whose magnetic moment is small (μ=-0.11 n.m.) and on the radioactive $J^\pi=7/2^+$ isomer that has a large moment of μ=4.4 n.m. (see upper left part of Fig. 8, and Sebastian et al. [97]). Subsequently, the βdn-activities were measured as a function of laser frequency for ^{122}Ag up to ^{127}Ag (see Fig. 8). All Ag isotopes show – apart from the expected small isotope shift – the same global pattern, where the moment of the odd $g_{9/2}$-proton is the dominant source of HF-splitting.

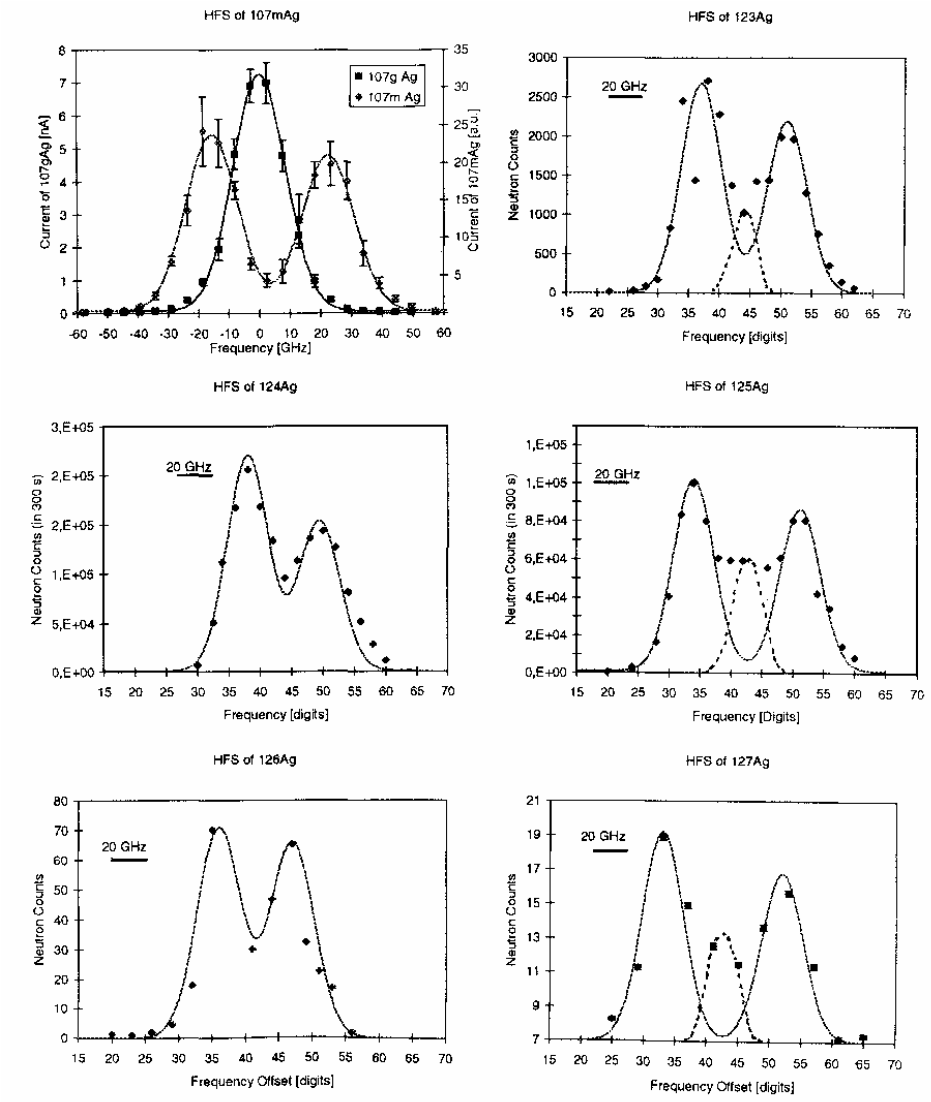

Figure 8. Laser frequency scans for ^{107}Ag and $^{123-127}$Ag using beam current or βdn-counting, respectively [55,94,97]. The global distributions of the short-lived radioactive isotopes are consistent with the typical HF-splitting of a $\pi g_{9/2}$ configuration. The odd-mass nuclei show in addition – as in the case of stable ^{107}Ag – a weak central peak indicating the $\pi p_{1/2}$ component.

For ^{122}Ag, previous decay-studies had already indicated the presence of both a low- and a high-spin isomer [98]. And indeed, apart from the highly split peak that can be associated with a $(\pi g_{9/2}{-}\nu h_{11/2})_{9^-}$ configuration, another narrow peak shows up in the center that could arise from the $(\pi p_{1/2}{-}\nu d_{3/2})_{1^-}$ configuration (see Fig. 9). Subsequently, both βdn- and γ-decay from ^{122}Ag was studied

as a function of laser frequency. As is evident from the partial γ-spectra shown in the lower part of Fig. 9, when the laser is set at the center of the frequency scale, γ-rays from both isomers can be observed. However, when the laser frequency is shifted away from the center (to 35 units), ionization of the low-spin isomer is suppressed, and the γ-spectrum indicates that only the decay of the high-spin isomer is oberved. Similarly, when following the βdn-decay curves as a function of laser frequency, different half-lives are obtained which represent varying admixtures of the two isomers. From a preliminary analysis, we get a half-life of the low-spin isomer of $T_{1/2}\simeq$550(50) ms and a value of $T_{1/2}\simeq$200(50) ms for the high-spin isomer of ^{122}Ag [94,99]. This experiment clearly demonstrates the sensitivity of ionization to laser frequency and marks the first spectroscopic application of this technique to short-lived isomers. In the meantime, a gross analysis of γ-spectra taken at different laser-frequency settings confirms isomerism also for the heavier Ag isotopes up to (at least) ^{126}Ag.

An important nuclear-physics quantity for r-process nucleosynthesis calculations (in particular for the r-matter flow through the A$\simeq$130 region and the $N_{r,\odot}$ peak shape) is the β-decay half-life of the N=82 waiting-point isotope ^{129}Ag, situated just below ^{130}Cd. QRPA calculations using different Q_β-values and SP wave functions resulted in decay rates between 15 ms and 170 ms [34,35,42]. This had left large uncertainties in the reproduction of the A$\simeq$130 peak (see Fig. 1 in [55], and also Fig. 4 in [100]).

Initial attempts [85] to observe the βdn-decay of ^{129}Ag, performed with the (broad-band) lasers centered with respect to the mean frequency for the stable $\pi p_{1/2}$ ^{107}Ag, had failed. After the observation of enhanced ionization of the $\pi g_{9/2}$ level at an off-center frequency, a new experiment was performed with the laser setting at the left $\pi g_{9/2}$ peak value observed for ^{127}Ag (see lowest right part of Fig. 8). This approach together with the microgating procedure [96] mentioned above, finally permitted the unambiguous identification of the βdn-decay from $\pi g_{9/2}$ ^{129g}Ag (see Fig. 10). The half-life of 46^{+5}_{-9} ms is in very good agreement with the recent QRPA prediction of 47 ms [42], but is lower than our old 'waiting-point requirement' of about 130 ms [35,100]. However, that estimate was based on the earlier half-life measurement of $T_{1/2}\simeq$195 ms for ^{130}Cd, and on the older r-process residuals $N_{r,\odot}$ of [101]. However, for a non-equilibrium r-process, or after the breakdown of the β-flow equilibrium, also the $T_{1/2}$ contribution from the $\pi p_{1/2}$ ^{129}Ag isomer would be of importance for the 'stellar' half-life. With the QRPA model of [44], it is possible to calculate the GT decay for such an isomer to $T_{1/2}\simeq$320 ms. When including an estimate for the expected first-forbidden strength (extrapolated from the decay of the $J^\pi=1/2^-$ isomer in isotonic ^{131}In), a minimum value of $T_{1/2}\simeq$125 ms is suggested. And, indeed, a careful re-examination and comparison of the A=129 βdn-decay curve taken with the laser at central frequency with the pure ^{129}In curve from a laser-off run, gave a first indication of a weak, 'longer-lived' ^{129}Ag βdn-component with a

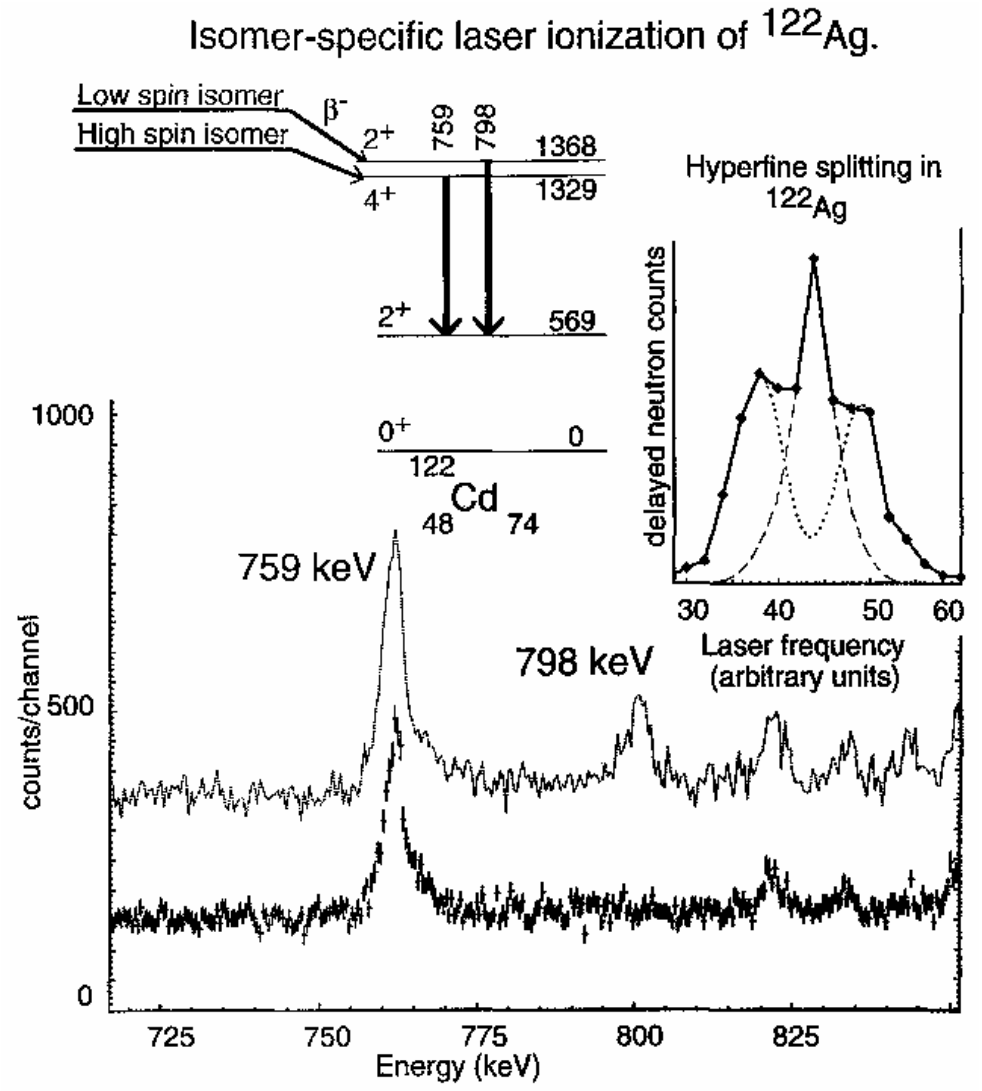

Figure 9. Portions of γ-ray spectra of the decay of ^{122}Ag isomers. The upper spectrum was taken with the laser frequency set at the center peak (44 units; see insert upper right part), and can be compared with the lower spectrum obtained at an off-center frequency (35 units). The γ-ray at 798 keV has been assigned to the $2_2^+ \rightarrow 2_1^+$ transition (see insert upper left part), whereas the line at 759 keV corresponds to the decay of the 4_1^+ level to the 2_1^+state [98].

half-life of roughly 160 ms.

Now, it will be important to use isomer-specific laser ionization in combination with isobar separation at ISOLDE-HRS to ascertain the existence of this $\pi p_{1/2}$ isomer. The astrophysical half-life of ^{129}Ag for non-equilibrium conditions, expected to be a mixture of the g.s and isomer values, might then lead to a better

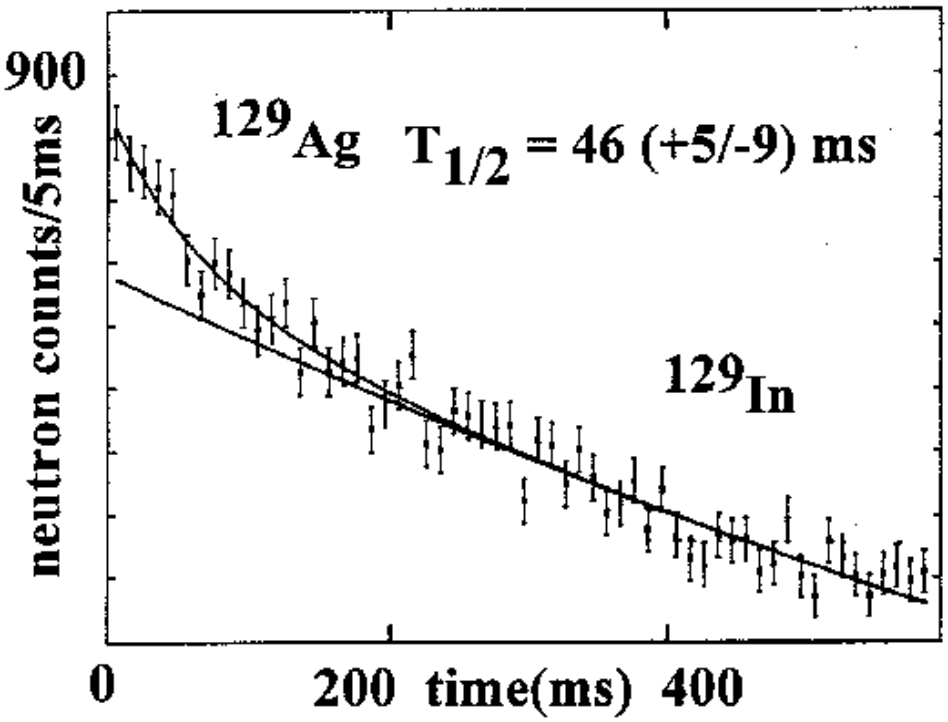

Figure 10. βdn-multiscaling curve for A=129. On top of the isobar activities from the two known ^{129}In isomers, which are due to surface ionization, the laser-ionized ^{129}Ag $\pi g_{9/2}$ g.s.-decay is shown.

understanding of the 'bottle-neck' behaviour and shape of the A$\simeq$130 $N_{r,\odot}$ peak. Based on our present knowledge on level systematics in the ^{132}Sn region, neutron-capture γ-decay from $S_n \simeq 5.6$ MeV in ^{129}Ag would populate the $\pi p_{1/2}$ isomer to roughly 35% and the $\pi g_{9/2}$ ground state to about 65 % [102]. This would result in an average stellar $T_{1/2} \simeq 80$ ms. However, already within the waiting-point approximation requesting only the $T_{1/2}$ of ^{129g}Ag, an excellent reproduction of the shape of the $N_{r,\odot}$ peak from A=126 to A=133 is obtained. From this result, we conclude that the effect of neutrino-processing of the $N_{r,prog}$ during freeze-out is considerably smaller for the A$\simeq$130 peak region than recently postulated by Qian et al. [103], and that the main effect is rather due to βdn-branching during the first 100 ms of the freeze-out.

In addition to the study of gross β-decay properties of neutron-rich Ag isotopes, also the level systematics of the Cd-daughters has been extended up to the r-process path [86,99,94]. First, an alternate source of nuclear structure for neutron-rich isotopes is the investigation of correlated γ-emission of complementary fragments of spontaneous-fission systems. Recent data from such studies have revealed surprisingly low 2^+ to 6^+ energies in ^{134}Sn (only two neutrons

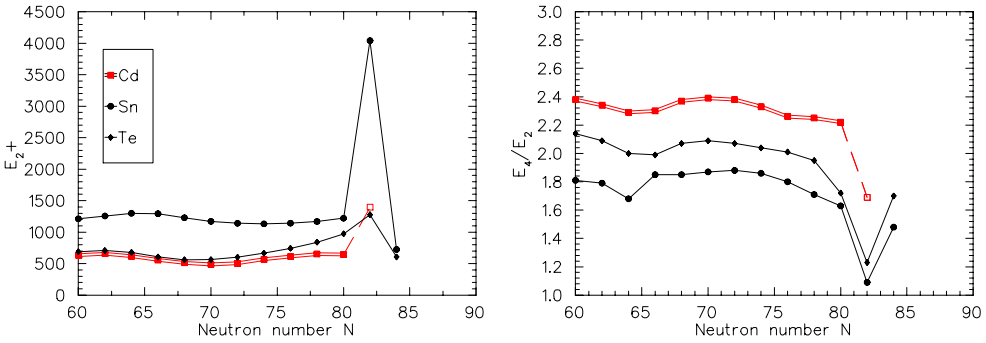

Figure 11. Systematics of the first 2^+ levels in neutron-rich $_{48}$Cd to $_{52}$Te isotopes (left part); and E(4^+)/E(2^+) ratios (right part).

beyond double-magic ^{132}Sn), that suggest a reduction of the effects of pairing in very neutron-rich Sn nuclides [104]. For the Cd isotopes, however, such fission data extend only up to ^{122}Cd. Our studies at ISOLDE have now permitted even-even Cd structures to be extended six neutrons further out, up to N=80 ^{128}Cd.

The new results are shown in Fig. 11, together with known E(2^+) and E(4^+)/E(2^+) level systematics of neighbouring even-Z elements. The E(4^+)/E(2^+) ratio for the 4n-hole nuclide ^{126}Cd is 2.25, a value almost unchanged relative to that for the 6n-hole isotope ^{124}Cd. Already this static ratio is in contrast to the larger reduction observed for the Z=52 isotones ^{128}Te and ^{130}Te. For the new 2n-hole nuclide ^{128}Cd, the energy of the first 2^+ state at 645 keV is even **lower** than the E(2^+) of 657 keV in ^{126}Cd, and also the E(4^+)/E(2^+) ratio of 2.22 is only insignificantly smaller than those in ^{124}Cd and ^{126}Cd. As can be seen from the right side of Fig. 11, this trend for the Z=48 isotopes clearly deviates from that of the Z=50 (Sn), 52 (Te) and 54 (Xe) isotones. This situation is similar to the Hg isotopes below N=126, where the E(2^+) in the 2n-hole nuclide $^{204}_{80}$Hg$_{124}$ is with 436.6 keV also slightly lower than the E(2^+)=439.6 keV in the 4n-hole isotope $^{202}_{80}$Hg$_{122}$. For the ee-Cd nuclides this indicates an extension of the well-known vibrational character of the lighter isotopes up to N=82, indicating a weakening of the spherical shell strength below ^{132}Sn. For A=130, we do have an indication for two weak γ-lines at 957 keV and 1395 keV with a tentative assignment to the 4^+ and 2^+ levels in ^{130}Cd. If confirmed, this would result in an E(4^+)/E(2^+) ratio of 1.69.

As the above results were accomplished with LIS and GPS-ISOLDE, again there is promise of additional data with HRS. In particular, a study of the decay of isobaric 'clean' ^{130}Ag should permit the identification of excited states of N=82 ^{130}Cd up to the 8^+ level in which two aligned $g_{9/2}$ proton holes are coupled to double-magic ^{132}Sn. As the structure of ^{98}Cd, which has the same two $g_{9/2}$ aligned protons coupled to the double-magic ^{100}Sn core, is known, a direct comparison is already available for such a measurment at N=82. There also exists the possibilty

of the presence of a low-spin $\pi p_{1/2}$ isomer in ^{131}Ag that should populate the $\nu p_{3/2}$ state in the ^{131}Cd-daughter. As has been mentioned previously, one possible effect of large neutron excess in nuclei is the lowering of the low-j orbitals. Hence, an HRS study of ^{131}Ag decay could demonstrate if the 854-keV gap between the $\nu p_{3/2}$ first excited state and the $\nu f_{7/2}$ g.s. in $^{133}Sn_{83}$ has narrowed with the removal of two protons in the N=83 Ag isotone.

Under development and testing at ISOLDE is a scheme for laser ionization of Sn nuclides [95]. If past experience is any guide, again, it should be possible with GPS and HRS to produce and study the decay of at least six Sn isotopes beyond ^{134}Sn, the heaviest Sn nuclide for which some nuclear properties are known. ^{140}Sn is a nucleus with 50 protons and 90 neutrons, a neutron/proton ratio of 1.8. It would be the most neutron-rich nuclide studied beyond the sd shell; and if there are to be strong divergences from expected nuclear properties because of the high neutron/proton ratio, the properties of this nuclide should reveal such signatures. Moreover, these heavy Sn nuclides lie directly in the path of the r-process, and the degree to which they capture neutrons prior to undergoing β-decay is a measure of how quickly the r-process flow can be established beyond the waiting-point nuclides at N=82. At this point, all nucleosynthesis calculations use predicted $T_{1/2}$ values which are presumably too long.

Given the recent, highly interesting results in the ^{132}Sn region, one is tempted to re-inspect existing data for additional 'hidden' or so far unrecognized signatures of shell quenching at N=82. And indeed, first qualitative evidence for such a phenomenon came already from a comparison of the old $T_{1/2}$ measurement of $^{130}Cd_{82}$ [39] with predictions from the original QRPA model of Möller and Randrup [44]. When applying Q_β-values from the 'unquenched' mass models FRDM [42] and ETFSI-1 [45], theoretical $T_{1/2}$ values for GT-decay of 1.12 s and 674 ms are obtained, respectively. However, with the 'quenched' mass formulae HFB/SkP [61] and ETFSI-Q [46], shorter values of 246 ms and 364 ms, respectively, are derived which are in better agreement with experiment. Another, so far unrecognized indication is given by the measured masses in the ^{132}Sn region [52,82]. As can be seen from Fig. 12, between the sequence of $_{50}$Sn and $_{48}$Cd isotopes there is a significant change in the trend of the experimental and theoretical mass differences (normalized to the FRDM predictions, M_i-M_{FRDM}). Clearly, for the Cd isotopic chain the best agreement with the measured masses is obtained with the 'quenched' ETFSI-Q.

All these signatures can, of course, only be taken as first evidence for a 'quenching' of the spherical N=82 shell below ^{132}Sn. Certainly, much more experimental data, including nuclear masses (and, as e.g. shown in Fig. 4 of [54], in particular S_n values of N=81 and 83 isotones), single-neutron levels, as well as spectroscopic factors of transfer and pickup reactions on radioactive isotopes around ^{132}Sn, are necessary to quantify the effect of shell quenching. As will be shown in the next section, a vanishing of the classical, spherical N=82 and 126

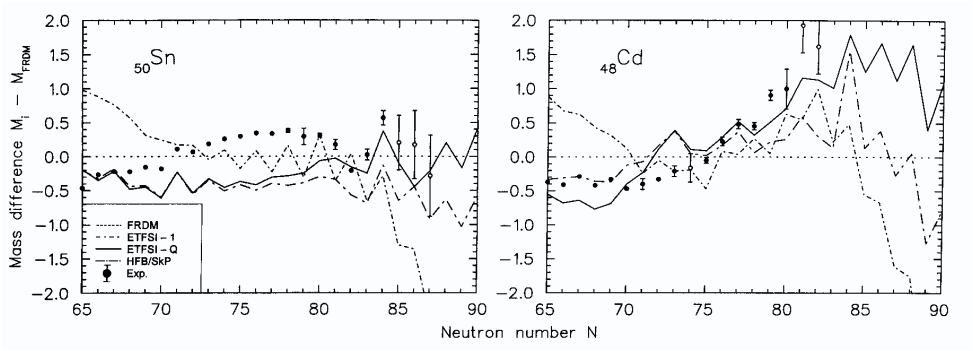

Figure 12. Experimental and theoretical mass differences for $_{50}$Sn and $_{48}$Cd isotopes normalized to FRDM values (M_i–M_{FRDM})

shell closures would not only be an interesting new nuclear-structure phenomenon close to the neutron drip-line, but may also have important consequences for r-process nucleosynthesis up to the Th, U, Pu cosmochronometers, and maybe even beyond (see, e.g. [105,106]).

5. Solar r-Process Abundances and Astrophysical Sites

5.1. Reproduction of the global $N_{r,\odot}$ pattern

Mainly as a result of the improved nuclear-physics input, our r-process parameter studies have revealed that the entire isotopic $N_{r,\odot}$ pattern cannot be reproduced by assuming a global steady flow. Instead, even in a single SN II event it requires a superposition of a multitude of components (minimum three) with different neutron densities or equivalenty different S_n's, characterizing different r-process paths and time scales. In our approach, the weighting of the individual r-components is naturally given by the β-decay half-lives of the three waiting-point nuclei ^{80}Zn, ^{130}Cd and ^{195}Tm which represent the (main) progenitors of the stable isobars ^{80}Se, ^{130}Te, ^{195}Pt situated at the top of the respective $N_{r,\odot}$ peaks. That this approach has, indeed, a nearly one-to-one mapping to 'realistic' astrophysical environments with time variations has been discussed in some detail in [35,54,13]. In Fig. 13, we show global N_r distributions from a superpostion of sixteen $n_n - \tau$ components for two versions of the ETFSI nuclear mass model (EFTSI-1 [45] and ETFSI-Q [46]). In both cases, identical conditions for the stellar parameters were used. Within this framework, the successful reproduction of the position and relative height of the $N_{r,\odot}$ peaks as well as the remaining defiencies have been interpreted as signatures of nuclear structure near the neutron drip-line [35,54–56]. It should be mentioned at this point, that this interpretation is in contradiction with the conclusions of other authors (see, e.g.

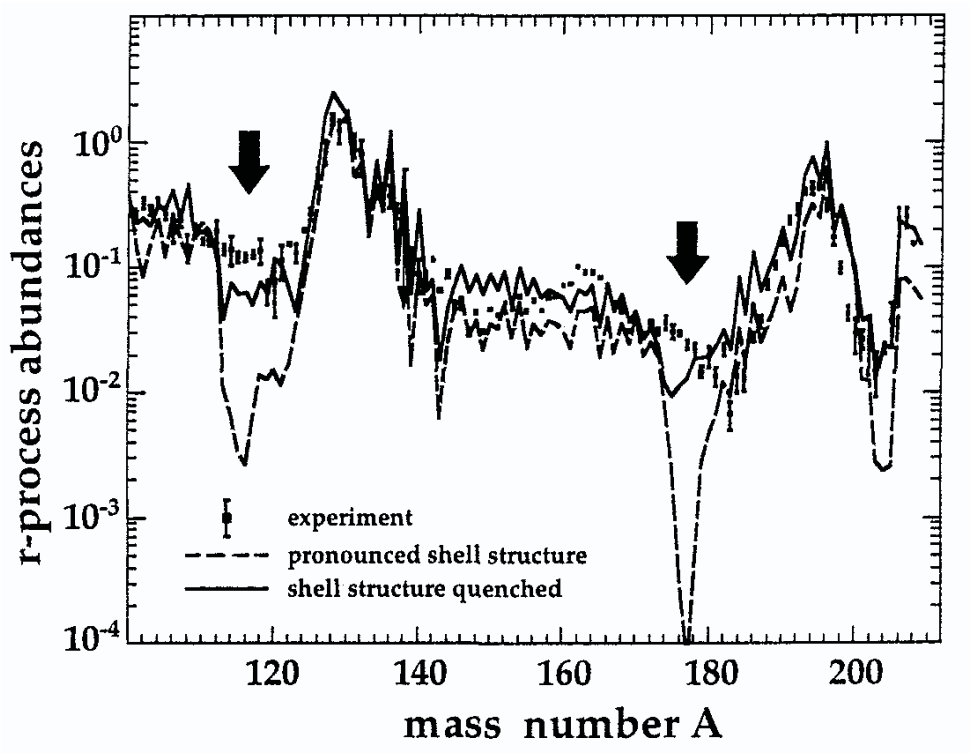

Figure 13. Global r-abundance fits for the ETFSI-1 mass model [45] with pronounced shell structure and the ETFSI-Q formula [46] with quenched shell gaps. For discussions, see text and [56,55].

[32]) who prefer a mathematical 'Fourier-type' analysis, assuming that the $N_{r,\odot}$ pattern represents a 'multi-SN-event' composition.

As can be seen from Fig. 13 (dotted fit-curve), with the ETFSI-1 mass model, apart from pronounced A≃115 and A≃175 abundance troughs, too little r-process material is observed in the whole region beyond the A≃130 peak. The solution to the A≃115 r-abundance deficiency clearly lies in the prediction of nuclear properties along the r-process path in this mass range, which have their origin in an overestimation of the N=82 shell strength below ^{132}Sn (for a more detailed discussion see [35]). Analogous deficiencies in describing shape-transitions around N≃104 midshell and the N=126 shell strength seem to be the origin of the deep A≃175 r-abundance trough.

It has therefore been suggested [35,38,100,54,56], that the trough problem might be resolved if for very neutron-rich nuclei the N=82 and 126 shell gaps are less pronounced than predicted by the global mass models [30,45] used so far in r-process calculations. A weakening of sperical shells near stability with increasing isospin, resulting in a gradual setting in of collectivity, is well established for the

N=20 and 28 shells (see, e.g. [107–109]), and is also indicated at N=50 [65,35]. Quenching of spherical shells at N=82 and 126 has recently been predicted by HFB calculations [47,110,111], and the infinite nuclear matter model [112].

In order to check our predictions, in a first step we have replaced the FRDM masses by the S_n's from the spherical HFB/SkP model [61] locally in the vicinity of the N=82 shell closure. With this, we could indeed observe a considerable improvement of the calculated r-abundances in the 'pathological' A≃115 region (for a more detailed discussion, see [54] and Figs. 2 and 3 therein). Motivated by this success, in a next step we have replaced the spherical HFB/SkP masses by the global ETFSI-Q model which takes into account both deformation and shell quenching [46]. The full curve in Fig. 13 shows the result of a multicomponent fit with the latter masses. When compared to the N_r curve obtained with the ETFSI-1 formula, a considerable improvement of the overall fit is observed. In particular the prominent abundance troughs in the A≃115 and 175 regions are eliminated to a large extent.

Hence, a 'quenched' mass model for r-abundance calculations beyond A≃110 seems to be highly recommended, especially if predictions for the A≥200 mass region are required. Of special interest in this context is the good agreement for the region between ^{203}Tl and ^{209}Bi with the recent $N_{r,\odot}$ evaluation of [37]. For ^{209}Bi, for example, it indicates a nearly pure r-process origin of this isotope, which confirms that (at least in the frame of the double-pulse s-process model) only a minor contribution to this isotope is of s-origin. As a consequence, there is no further need for the so-called 'strong' s-process component, which had been introduced originally to account for the Pb and Bi abundances.

This improvement with the ETFSI-Q masses should also make extrapolations up to the progenitors of the long-lived actinides ^{232}Th and ^{235,238}U more reliable, in particular since they are for the first time based on an internally consistent nuclear-physics input. For galactic-age determinations, commonly production ratios of cosmochronometers, in particular ^{232}Th/^{238}U, are applied. In [56], we have compared the results derived from different mass models to literature values. Only when using nuclear masses which correctly describe the entire $N_{r,\odot}$ pattern, consistent values for a Galactic age of 10-14 Gyrs could be obtained when following the procedure described in [7].

5.2. An ultra-metal-poor, neutron-capture-rich halo star

Recently, Sneden et al. [113] have determined elemental abundances of 17 heavy elements between Ba and Th for the ultra-metal-poor, neutron-capture-rich halo star CS 22892–052. In Fig. 14, these values are compared to the solar r-element distribution and to our ETFSI-Q predictions, after adjustment to the solar metallicity. The very good agreement clearly indicates, that the heavy elements in this star are of pure r-process origin. With the above measured Th abundance and our calculated initial abundance, a lower limit for the age of this

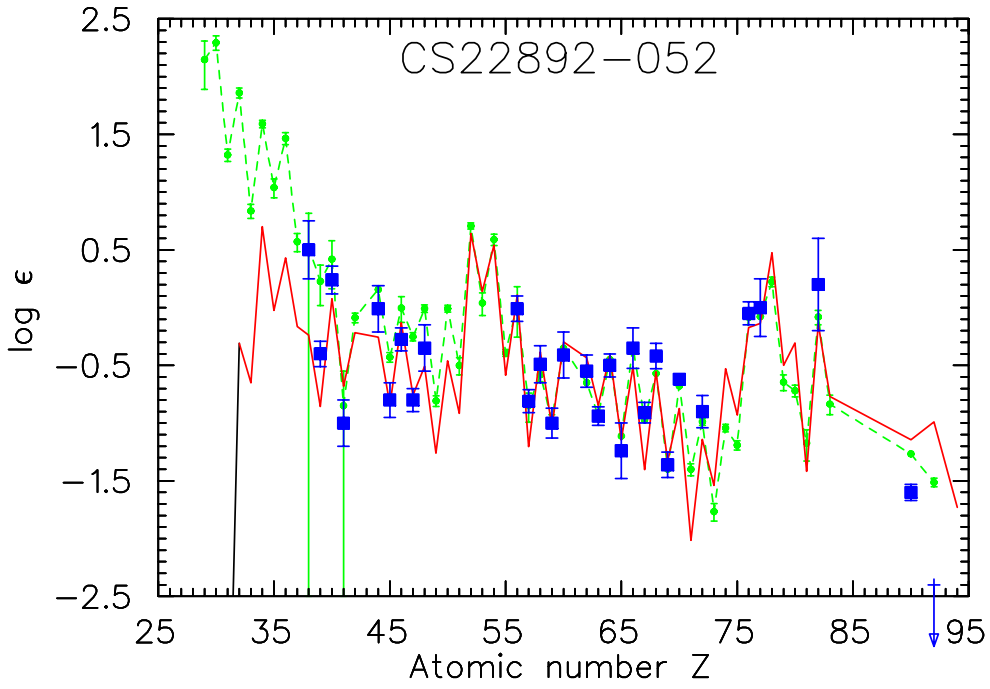

Figure 14. Elemental r-abundances in units of log ϵ calculated with ETFSI-Q (full line) are compared to the respective $N_{r,\odot}$ values (filled circles, connected by dashed line). Superimposed are measured abundances (filled squares) from the metal-poor halo star CS 22892–052 [113,115], which were normalized to the solar rare-earth values.

star can be deduced when normalizing to a stable r-only element, e.g. Eu. From the observed ratio Th/Eu=0.219 in this halo star, combined with our ETFSI-Q prediction of Th/Eu=0.480 for the initial ratio, a lower limit of its 'decay age' of 14.5 Gyrs is obtained [105], which overlaps with recent Galactic ages on the young side (see, e.g. [114]). This implies that the heavy elements in CS 22892–052 must have been synthesized already very early in the Galactic evolution, prior to the onset of s-process nucleosynthesis [113,105]. Finally, the excellent agreement between the r-element abundances of this first-generation star and the global $N_{r,\odot}$ pattern, which represents a summation over the whole Galactic evolution, indicates that there is probably a *unique* scenario for the r-process beyond A$\simeq$130. In the meantime confirmed by observations of other metal-poor stars [14,105], this result seems to validate our deductive approach of deducing unique astrophysical constraints on r-process conditions from fitting the global $N_{r,\odot}$ abundances.

Only a few months ago, Cowan et al. [115] have presented new element-abundance data for the halo-star CS 22892-052 obtained at the Keck I high-resolution spectrograph. They partly supercede the earlier analysis of the same group [113], and in addition give first results on the abundances between $_{41}$Nb

and $_{48}$Cd. An interesting feature of the latter element pattern is the pronounced odd-even-Z staggering. All observed odd-Z elements below Z=50 ($_{39}$Y, $_{41}$Nb, $_{45}$Rh and $_{47}$Ag) are clearly under-abundant compared to the (metallicity-scaled) solar pattern, whereas the even-Z elements ($_{40}$Zr, $_{44}$Ru, $_{46}$Pd and $_{48}$Cd) are – within the given errors – only slightly under-abundant (see Fig. 14). These new 'low-Z' data seem to support the recent evidence for a two-source nature of the solar r-process, originally concluded from extinct radioactivities ($1.57{\cdot}10^7$-y ^{129}I and $9{\cdot}10^6$-y ^{182}Hf) in meteorites [116].

Taking advantage of our 'site-independent', exponential multicomponent approach to fit the $N_{r,\odot}$ pattern, we now can test within the waiting-point assumption under which stellar conditions (mainly neutron density and process duration) the possible two r-processes have to run, in order to reproduce the 'low-Z' (below Z$\simeq$50) and 'high-Z' (beyond Z$\simeq$50) element-abundances of CS 22892-052.

When assuming that the abundances of this extremely old metal-poor halo star are a living record of the first (few) generation(s) of Galactic nucleosynthesis [105], the observed pattern beyond Zr up to Th (the trend of the lighter elements up to Zr may be explainable in terms of the weak s-process) should most likely be produced by only **one** r-process site. This scenario (the *'main'* r-process) then produces the 'low-Z' elements under-abundant compared to solar, and reaches the solar r-pattern presumably beyond $_{48}$Cd. Fig. 14 shows a fit to the recent CS 22892-052 data, using our standard multicomponent approach [35,56,105] with the ETFSI-Q nuclear masses. The trend for the 'low-Z' elements – pronounced odd-even staggering, and approaching the solar values with increasing Z – is nicely reproduced, and the good overall reproduction of the 'high-Z' elements (beyond $_{56}$Ba) is maintained. When starting from an Fe-group seed, this requires a **minimum** neutron density of $n_n \geq 10^{23}$ cm^{-3} in order to simulate the observed partial 'drying-out' of the r-matter flow at low Z. In terms of radiation entropy within the realistic scenario of the high-entropy wind in SNII (see sect. 5.3), this would translate to S$\geq$200 k_B for Y_e=0.45 [13]. As a consequence of the present observations for CS 22892-052 (but also for other halo stars) and our calculations, the 'residuals' at low Z relative to the solar distribution, i.e. $N_{r,\odot}$ - $N_{r,main}$, will require a separate *'weak'* r-process component of yet unknown stellar site. Again, when assuming an Fe-group seed, our calculations can reproduce also the resulting $N_{r,weak}$ pattern up to $_{47}$Ag for neutron densities of $10^{20} \leq n_n \leq 10^{22}$ at T_9=1.35 and a process duration of $\tau \simeq 1.5$ s. A choice of $_{40}$Zr as seed (in order to avoid the delay in the A$\simeq$80 bottle-neck region), would speed up the low-Z production to $\tau \simeq 0.5$ s. These are conditions that might be reached in explosive shell-burning scenarios (see e.g. [117]). But, before being able to draw more definite conclusions, considerably more work has to be done in both astrophysics (site, seed, n_n,...) and nuclear physics (masses, β-decay properties, shell-quenching at N=50).

5.3. Astrophysical Sites

After having tested nuclear properties with a site-independent approach in the previous subsection, we want to return briefly to the possible astrophysical r-process sites introduced already in section 1.2, i.e. SNII and neutron-star (NS) mergers. In the first case, a wind of matter from the neutron star surface (within seconds after a successful supernova explosion) is driven via neutrinos streaming out from the still hot neutron star [11,12,28,29,118,119]. This high entropy 'neutrino wind' (corresponding to conditions plotted in the left part of Fig. 1) is leading to a superposition of ejecta with varying entropies. An abundance pattern resulting from a superposition of such high-entropy environments, representing α-rich freeze-outs of various degrees, is shown in Fig. 15 [13]. The high entropies (up to 400 k_b/nucleon, responsible for the mass region A>110) reproduce nicely the $N_{r,\odot}$ pattern, with the exception of the mass region 110–120, where the same conclusions can be drawn as in the site-independent studies (see sect. 5.1). The trough is the result of the nuclear-structure deficiencies of the ETFSI-1 mass model below N=82. The lower entropies are responsible for the abundances in the mass region 80–110. We see that the predictions for that region do not reproduce the solar r-abundances. The reason is that essentially no neutrons are left after an α-rich freeze-out with such entropies, and the abundance pattern is dictated by α-separation rather than neutron-separation energies. Thus, explaining the r-process by ejecta of SNII faces two difficulties: (i) whether the required high entropies for reproducing heavy r-process nuclei can really be attained in supernova explosions has still to be verified, (ii) the mass region 80–110 cannot be reproduced adequately. It has to be seen, for example, whether the inclusion of non-standard neutrino properties [120] can cure both difficulties. Given the galactic occurence frequency, SNII would need to eject about 10^{-5} $M_\odot$ per event.

An alternative site are neutron-star mergers. Interest in a scenario where a binary system, consisting of two neutron stars (NS-NS binary), looses energy and angular momentum through the emission of gravitational waves comes from various sides. Such systems are known to exist; five NS-NS binaries have been detected by now [121]. The measured orbital decay gave the first evidence for the existence of gravitational radiation [122]. Further interest in the inspiral of a NS-NS binary arises from the fact that it is the prime candidate for a detection by the gravitational wave detector facilities that will come into operation in the very near future. A merger of two NS may also lead to the ejection of neutron-rich material, and could be a promising site for the production of r-process elements. It is even possible that such mergers account for *all* heavy r-process matter in the Galaxy [16,18,19]. The decompression of cold neutron-star matter has been studied [16,17]; however, a hydrodynamical calculation coupled with a complete r-process calculation has not been undertaken, yet.

Fig. 16 shows the composition of ejecta from a NS merger with an assumed superposition of components with Y_e=0.08-0.14, as expected when an average of

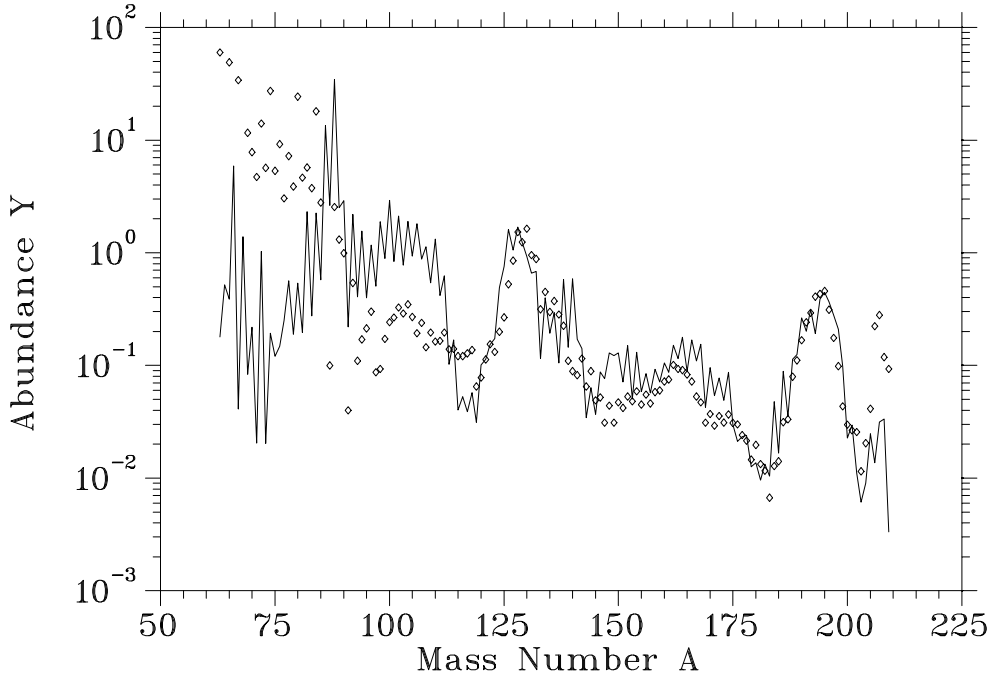

Figure 15. Fit to solar r-process abundances $N_{r,\odot}$ (open rhombus) with the ETFSI-1 mass formula [45], making use of a superposition of entropies $g(S)$ from the high-entropy neutrino wind in SNII. These calculations were performed with $Y_e = 0.45$, but similar results are obtained in the range $0.30 - 0.49$, only requiring a scaling of entropy. The trough below $A \simeq 130$ behaves similar to Fig. 13, and can be avoided by the quenching of shell effects. The strong deficiencies in the abundance pattern below $A \simeq 110$ are due to the α-rich freeze-out and thus related to the astrophysical scenario rather than to nuclear structure from [13]).

spin orientation in merger events is taken [123]. It is seen that the large amount of free neutrons (up to $n_n \simeq 10^{32}$ cm^{-3}) available in such a scenario leads to the build-up of the heaviest elements and also to fission cycling within very short timescales, while the flow from the Fe-group to heavier elements 'dries out'. This leads to a complete composition void of abundances below the A$\simeq$130 peak. If this tendency is confirmed, e.g. by further observations of Z$<$50 elements in very low metallicity stars, it would provide strong support for that r-process site, but would definitely require an additional astrophysical source which produces the bulk of the lighter r-abundances up to A$\simeq$125.

The rate of NS mergers has been estimated to be of the order $10^{-6} - 10^{-5}$y^{-1} per galaxy [18,124]; more recent estimates [125] tend towards the higher end of this range ($8 \cdot 10^{-6}$y^{-1} per galaxy). Hydrodynamic simulations of NS mergers are a formidable task. Beyond 3D hydrodynamics, it should include general relativistic effects, employ a realistic equation of state, contain neutrino transport and neutrino cooling, as well as all possible nuclear reactions [126–129]. We [19,123] have performed extensive NS-NS merger calculations and find typically ejecta

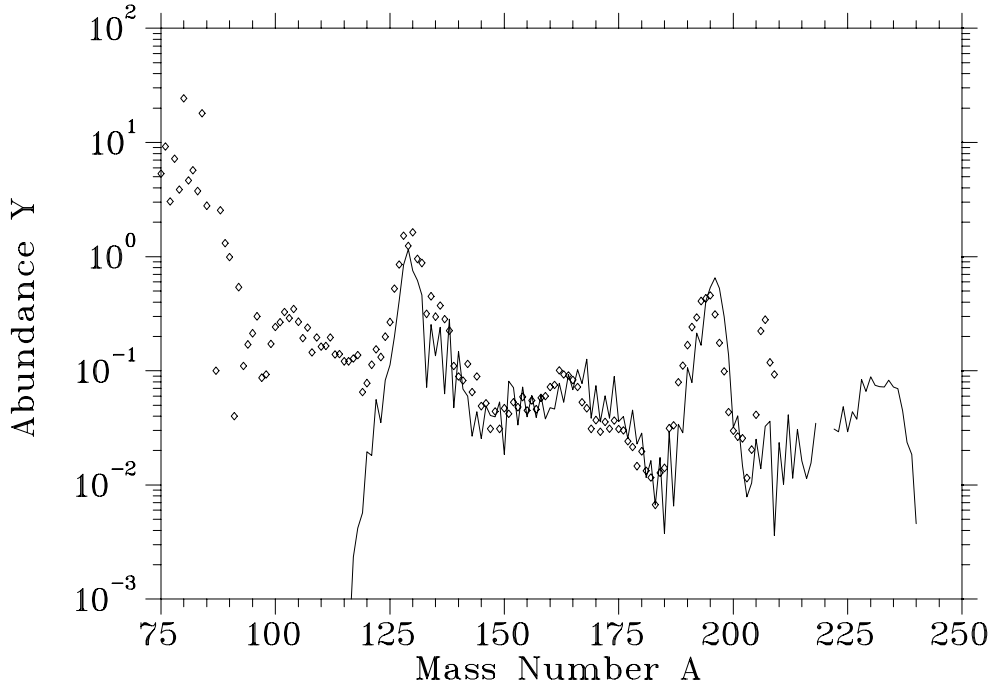

Figure 16. Composition of ejecta from a neutron star merger event with an assumed superposition of components with Y_e=0.08-0.14, as expected when an average of spin orientation in NS merger events is taken. For discussion, see text.

of the order 10^{-2}M$_\odot$. This is sufficient to reproduce the solar system r-process abundances, provided that this matter is converted into an r-process abundance pattern (which still needs to be shown).

6. Conclusion

We have shown in this review which nuclear properties are of prime importance in the astrophysical r-process. Due to the (partial) equilibrium nature at high temperatures and neutron densities, the major aspects to explore are nuclear masses and β-decay properties (half-lives, delayed neutron emission and fission). The application of recent experimental findings to 'site-independent' r-process calculations has shown that the N$_{r,\odot}$ abundances actually bear the possibility to test the evolution of nuclear structure and shell effects as a function of the distance from β-stability. In order to put these indications on a more solid footing, the experiments have to be extended further towards the neutron drip line, which sets strong requirements for future beam intensities and thus target techniques as well as experimental methods. Innovation has played a strong part in establishing a premier role for ISOLDE in the study of properties of nuclides very far from stability. The development of the techniques of laser ionization is one example

of this kind of innovation. A strong lesson from LIS work is that *selectivity* is the key to extending the current results to even more exotic nuclides. Ultimately, the combination of Z-selective laser ionization, isomer separation via HF-splitting and the use of the HRS for isobar separation promises enhanced selectivity.

Astrophysical knowledge is not at all in a more advanced stage. We have presented two 'realistic' sites for the r-process, (i) supernovae of type II and (ii) neutron star mergers, which represent the two options to obtain a high neutron to seed-nuclei ratio: high entropies with moderate Y_e or neutron to proton ratios, or low entropies with small Y_e or high neutron to proton ratios.

The first scenario is (as is the SN explosion mechanism) still riddled with the question whether the required high entropies of more than 200 k_B per nucleon can be attained at all and that the lower entropy components give rise to the over-production of non-solar r-patterns in the mass range A$\simeq$80–110. Possibly only exoctic neutrino properties (like sterile neutrinos) might save this environment.

The NS mergers could overcome these problems, if the amount of ejected matter stays the same in models with general relativity [19], and a statistical average over neutron-star spins permits that matter in the range of Y_e=0.1 is predominantly ejected [123,130]. An interesting feature of the second environment is that nuclei with masses below the A$\simeq$130 peak are essentially unproduced (see Fig. 16).

The fact that both scenarios are unable to reproduce the $N_{r,\odot}$-'residuals' in the A$\simeq$80–120 region, might be related to the increasing evidence of a two-source nature of the solar r-process, which was recently concluded from extinct radioactivities in meteorites [116] and the low abundances of the odd-Z elements $_{39}$Y to $_{47}$Ag measured in CS22892-052 [115], and in other low-metallicity stars (which show for all elements heavier than Ba (Z=56) a solar r-process pattern [113,131,115]). Further detailed observations of r-process abundances in low-metallicity stars, especially for A<130 are highly needed for uncovering the nature and stellar site of this second (*'weak'*) r-process and fixing the time in galactic evolution when this nucleosynthesis process sets in.

Acknowledgement

The authors wish to acknowledge collaboration with many colleagues, in particular P. Möller, J. Dobaczewski, J.M. Pearson, B.A. Brown, W. Hillebrandt, J.W. Truran, Ch. Freiburghaus, T. Rauscher, S. Rosswog, J.J. Cowan, V.N. Fedoseyev, V.I. Mishin, H. Gabelmann, G. Lhersonneau, A. Wöhr, W. Böhmer, H.L. Ravn and the ISOLDE Collaboration, and all our present and former PhD students and postdocs. Support for this work was provided by various grants from the German BMBF and DFG, the Swiss Nationalfonds and U.S. DOE.

References

[1] E.M. Burbidge et al., Rev. Mod. Phys. 29 (1957), 547.
[2] A.G.W. Cameron, Atomic Energy of Canada, Ltd., CRL-41 (1957).
[3] P.A. Seeger et al., Ap. J. Suppl. 97 (1965), 121.
[4] A.G.W. Cameron et al., CERN, 70-30 (1970), 735.
[5] W. Hillebrandt, Space Sci. Rev. 21 (1978), 639.
[6] G.J. Mathews and R.A. Ward, Rep. Prog. Phys. 48 (1985), 1371.
[7] J.J. Cowan et al., Phys. Rep. 208 (1991), 267.
[8] F.-K. Thielemann et al., in: *Nuclear and Particle Astrophysics*, Cambridge University Press (1998), 27; available via WWW at URL: http://xxx.lanl.gov/astro-ph/9802077
[9] G. Wallerstein et al., Rev. Mod. Phys. 69 (1997), 995.
[10] F. Käppeler et al., Ann. Rev. Nucl. Part. Sci. 48 (1998), 175.
[11] S.E. Woosley et al., Ap. J. 433 (1994), 229.
[12] K. Takahashi et al., A&A 286 (1994), 857.
[13] C. Freiburghaus et al., Ap. J. 516 (1999), 381.
[14] A. McWilliam et al., A. J. 109 (1995), 2757.
[15] A. McWilliam, Ann. Rev. Astron. Astrophys. 35 (1997), 503.
[16] J.M. Lattimer et al., Ap. J. 213 (1977), 225.
[17] B. S. Meyer, Ap. J. 343 (1989), 254.
[18] D. Eichler et al., Nature 340 (1989), 126.
[19] S. Rosswog et al., A&A 341 (1999), 499.
[20] S.E. Woosley et al., Ap. J. Suppl. 26 (1973), 231.
[21] W.R. Hix and F.-K. Thielemann, Ap. J. 460 (1996), 869.
[22] W.R. Hix and F.-K. Thielemann, Ap. J. 511 (1999), 862.
[23] R.D. Hoffman et al., Ap. J. (August 1999), in press.
[24] F.-K. Thielemann et al., Ap. J. 460 (1996), 408.
[25] H. Schatz et al., Phys. Rep. 294 (1998), 167.
[26] F. Rembges et al., Ap. J. 484 (1997), 412.
[27] S.E. Woosley and R.D. Hoffman, Ap. J. 395 (1992), 202.
[28] R.D. Hoffman et al., Ap. J. 460 (1996), 478.
[29] R.D. Hoffman et al., Ap. J. 482 (1997), 951.
[30] P. Möller et al., At. Data Nucl. Data Tables 59 (1995), 185.
[31] A.G.W. Cameron et al., Astrophys. Space Sci. 91 (1983), 235.
[32] V. Bouquelle et al., A&A 305 (1996), 1005.
[33] K.-L. Kratz et al., J. Phys. G 14 (1988), 331.
[34] K.-L. Kratz, Rev. Mod. Astronomy 1 (1988), 184.
[35] K.-L. Kratz et al., Ap. J. 402 (1993), 216.
[36] F. Käppeler et al., Rep. Prog. Phys. 52 (1989), 945.
[37] H. Beer et al., Ap. J. 474 (1997), 843.
[38] F.-K. Thielemann et al., Nucl. Phys. A570 (1994), 329c.
[39] K.-L. Kratz et al., Z. Phys. A325 (1986), 489.
[40] E. Lund et al., Phys. Scr. 34 (1986), 614.
[41] R.L. Gill et al., Phys. Rev. Lett. 56 (1986), 1874.
[42] P. Möller et al., At. Data Nucl. Data Tables 66 (1997), 131.
[43] J. Krumlinde and P. Möller, Nucl. Phys. A417 (1984), 419.
[44] P. Möller and J. Randrup, Nucl. Phys. A514 (1990), 1.
[45] Y. Aboussir et al,. At. Data Nucl. Data Tables, 61 (1995), 127.
[46] J.M. Pearson et al., Phys. Lett. B387 (1996), 455.
[47] J. Dobaczewski et al., Phys. Rev. Lett. 72 (1994), 981.
[48] J. Dobaczewski et al., Phys. Scr. T56 (1995), 15.

[49] W.D. Myers, At. Data Nucl. Data Tables 17 (1976), 411.
[50] H. von Groote et al., At. Data Nucl. Data Tables 17 (1976), 418.
[51] K. Takahashi et al., At. Data Nucl. Data Tables 12 (1973), 101.
[52] G. Audi et al., Nucl. Phys. A624 (1997), 1.
[53] K.-L. Kratz et al., $T_{1/2}$ and P_n evaluation, KCh Mainz Report (1998).
[54] B. Chen et al., Phys. Lett. B355 (1995), 37.
[55] K.-L. Kratz et al., Nucl. Phys. A630 (1998), 352c.
[56] B. Pfeiffer et al., Z. Phys. A357 (1997), 235.
[57] C. Freiburghaus et al., Nucl. Phys. A621 (1997), 405c.
[58] K.L. Kratz et al., Il Nuovo Cimento A111 (1998), 1043.
[59] T. Tachibana et al., Progr. Theor. Phys. 84 (1990), 641.
[60] E.R. Hilf et al., Suppl. to Proc. Int. Conf. NFFS-3, CERN 76-13 (1976), 142.
[61] J. Dobaczewski et al., Phys. Rev C53 (1996), 2809.
[62] B.S. Meyer et al., Ap. J. 399 (1992), 656.
[63] K.-L. Kratz et al., Z. Phys. A340 (1991) 419.
[64] K.-L. Kratz et al., Z. Phys. A336 (1990) 357.
[65] K.-L. Kratz et al., Phys. Rev. C38 (1988), 278.
[66] *Proc. Nuclear Structure of the Zirconium Region*, Res. Rep. in Phys., Springer, ISBN 0-387-50120-7 (1988).
[67] *Proc. Nuclei Far From Stability / Atomic Masses and Fundamental Constants 1992*, Inst. of Phys. Conf. Ser. 132, IOP, ISBN 0-7503-0262-3 (1993).
[68] *Proc. Exotic Nuclei and Atomic Masses ENAM95*, Edition Frontières, ISBN 2-86332-186-2 (1995).
[69] S. Schoedder et al., Z. Phys. A352 (1995), 237.
[70] T. Mehren et al., Phys. Rev. Lett. 77 (1996), 458.
[71] G. Lhersonneau et al., Eur. Phys. J. A1 (1998), 285.
[72] *Exotic Nuclei and Atomic Masses - ENAM98*, Bellaire, USA; AIP Conf. Proc. 455 (1998).
[73] S. Franchoo et al., Phys. Rev. Lett. 81 (1998), 3100.
[74] O. Sorlin et al., Nucl. Phys. A632 (1998), 205.
[75] R. Grzywacz et al., Phys. Rev. Lett. 81 (1998), 766.
[76] M. Hannawald et al., Phys. Rev. Lett. 82 (1999), 1391.
[77] S. Raman et al., Phys. Rev. C43 (1991), 556.
[78] O. Sorlin et al., submitted to Nucl. Phys. A
[79] F. Azaiez and O. Sorlin, Nucl. Phys. News 8 (1998), 34.
[80] P. Hoff et al., Phys. Rev. Lett. 77 (1996), 1020.
[81] M. Sanchez-Vega et al., Phys. Rev. Lett. 80 (1998), 5504.
[82] B. Fogelberg et al., in: *Exotic Nuclei and Atomic Masses - ENAM98*, AIP Conf. Proc. 455 (1998), 502, 552, 785.
[83] N.J. Stone et al., Phys. Rev. Lett. 78 (1997), 820.
[84] C.T. Zhang et al., Z. Phys. A358 (1997), 9.
[85] V.N. Fedoseyev et al., Z. Phys. A353 (1995), 9.
[86] T. Kautzsch et al., Phys. Rev. C54 (1996), 2811.
[87] K.-L. Kratz et al., in: *Fission and Properties of Neutron-Rich Nuclei*, World Scientific, (1999), in print.
[88] T. Rauscher et al., Phys. Rev. C57 (1998), 2031.
[89] I. Ragnarsson and R.K. Sheline, Phys. Scr. 29 (1984), 385.
[90] W.B. Walters, in: *Fission and Properties of Fission-Product Nuclides*, AIP Conf. Ser. 447 (1998), 196.
[91] Jing-ye Zhang et al., Phys. Rev. C58 (1998), 2663.
[92] N. Erdmann et al., Appl. Phys. B66 (1998), 431.

[93] M. Hannawald et al., to be published.
[94] K.-L. Kratz, in: *Exotic Nuclei and Atomic Masses - ENAM98*, AIP Conf. Proc. 455 (1998), 827.
[95] V.I. Mishin et al., Nucl. Instr. Meth. Phys. Res. B73 (1993), 550.
[96] Y. Jading et al., Nucl. Instr. Meth. Phys. Res. B126 (1997), 76.
[97] V. Sebastian et al., in: *Exotic Nuclei and Atomic Masses - ENAM98*, AIP Conf. Proc. 455 (1998), 126.
[98] N.V. Zamfir et al., Phys. Rev. C51 (1995), 98.
[99] T. Kautzsch, PhD Thesis, Univ. Mainz; and to be published.
[100] K.-L. Kratz, in: *Nuclei in the Cosmos III*, AIP Conf. Proc. 327 (1995), 113.
[101] G. Walter et al., A&A 167 (1986), 186.
[102] T. Rauscher (1998), private communication.
[103] Y.-Z. Qian et al., Ap. J. 494 (1998), 285.
[104] C.T. Zhang et al., Z. Phys. A358 (1997), 9.
[105] J.J. Cowan et al., Ap. J. 521 (1999), in press; available via WWW at URL: http://xxx.lanl.gov/astro-ph/9808272
[106] A.J. Westphal et al., Nature 396 (1998), 50.
[107] N.A. Orr et al., Phys. Lett. B258 (1991), 29.
[108] O. Sorlin et al., Phys. Rev. C47 (1993), 2491.
[109] T.R. Werner et al., Phys. Lett. B333 (1994), 303.
[110] J. Dobaczewski, in: *Extremes of Nuclear Structure*; GSI, ISSN 0720-8715 (1996), 214.
[111] B.A. Brown, Phys. Rev. C58 (1998), 220.
[112] L. Satpathy and R.C. Nayak, J. Phys. G: Nucl. Part. Phys. 24 (1998),1527.
[113] C. Sneden et al., Ap. J. 467 (1996), 819.
[114] M. Salaris and A. Weiss, A&A 327 (1997), 107.
[115] J.J. Cowan et al., 1999, 194th AAS Meeting, Chicago, #67.04
[116] G.J. Wasserburg et al., Ap. J. 466 (1996), L109.
[117] F.-K. Thielemann et al., A&A 74 (1979), 175.
[118] Y.-Z. Qian and S. E. Woosley, Ap. J. 471 (1996), 331.
[119] B.S. Meyer et al., Phys. Rev. C58 (1998), 3696.
[120] G.C. McLaughlin et al., Phys. Rev. C (1999), in press.
[121] S.E. Thorsett, Phys. Rev. Lett. 77 (1996), 1432.
[122] J. Taylor, Rev. Mod. Phys. 66 (1994), 711.
[123] S.K. Rosswog et al., A&A, submitted
[124] R. Narayan et al., Ap. J. 395 (1992), L83.
[125] E.P.J. van den Heuvel and D.R. Lorimer, MNRAS 283 (1996), L37.
[126] M.B. Davies et al., Ap. J. 431 (1994), 742.
[127] H.T. Janka and M. Ruffert, A&A 307 (1996), L33.
[128] M. Ruffert and H.-T. Janka, A&A 338 (1998), 535.
[129] T.W. Baumgarte et al., Phys. Rev. Lett. 79 (1997), 1182.
[130] C. Freiburghaus et al., in preparation
[131] J.J. Cowan et al., Ap. J. 480 (1997), 246.